Ministry of Higher Education and Scientific Research
University of Baghdad
Institute of Laser for Postgraduate Studies

Refractive Index Sensor Based On Coreless fiber - Mach Zehnder Interferometer Structure

A Thesis Submitted to the Institute of Laser for Postgraduate Studies/ University of Baghdad in Partial Fulfillment of Requirements for the Degree of Master of Science in Laser/ Electronic and Communication Engineering

By
Saif Akeel Mohammed

B.Sc. Laser and Optoelectronics Engineering –2008

Supervisor
Prof. Dr. Abdul Hadi Al-Janabi

2017 AD   **1439 AH**

بسم الله الرحمن الرحيم

اللَّهُ نُورُ السَّمَوَاتِ والأرضِ مَثَلُ نُورِهِ كَمِشْكَاةٍ فِيهَا مِصْبَاحٌ الْمِصْبَاحُ في زُجَاجَةٍ الزُّجَاجَةُ كَأَنَّهَا كَوْكَبٌ دُرِّيٌّ يُوقَدُ مِن شَجَرَةٍ مُّبَارَكَةٍ زَيْتُونَةٍ لاَّ شَرْقِيَّةٍ وَلاَ غَرْبِيَّةٍ يَكَادُ زَيْتُهَا يضيءُ وَلَوْ لَمْ تَمْسَسْهُ نَارٌ نُّورٌ عَلَى نُورٍ يَهْدِي اللَّهُ لِنُورِهِ مَن يشاء وَيَضْرِبُ اللَّهُ الأمثال لِلنَّاسِ وَاللَّهُ بِكُلِّ شيء عَلِيمٌ ﴿٣٥﴾

صدق الله العظيم

CERTIFICATION

I certify that this thesis was prepared under my supervision at the Institute of Laser for Postgraduate Studies, University of Baghdad, as a partial fulfillment of requirements for the degree of "Master of Science in Laser/Electronic and Communication Engineering.

Signature:

Name: **Dr. Abdul Hadi Al-Janabi**

Title: **Professor**

Address: Institute of Laser for Postgraduate studies,

University of Baghdad.

Date: /   / 2017

(Supervisor)

In view of the available recommendation, I forward this thesis for debate by Examining Committee.

Signature:

Name: **Asst. Prof. Dr. Shelan Khasro Tawfeeq**

Title: Head of the Scientific Committee.

Address: Institute of Laser for Postgraduate studies,

University of Baghdad.

Date: 17/9 / 2017

Examination Committee Certification

We certify that we have read this thesis **"Refractive Index Sensor Based On Coreless fiber - Mach Zehnder Interferometer Structure"** and as Examination Committee we examined the student in its content and in our opinion it is adequate with standards as a thesis for the degree of Master of Science in Laser /Electronic and Communication Engineering.

Signature:

Name: **Dr. Mohamed K. Dhahir**

Title: Assistant Professor

Address: Institute of Laser for Postgraduate Studies/ University of Baghdad

Date: 21 /1 /2018.

(Chairman)

Signature:

Name: **Dr. Anwaar A. Al-Dergazly**

Title: Assistant Professor

Address: College of Engineering/ Al-Nahrain University

Date: / /2018.

(Member)

Signature Hanan
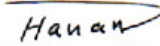
Name:. **Dr. Hanan J.Taher**

Title: Assistant Professor

Address: Institute of Laser for Postgraduate Studies/ University of Baghdad

Date: / /2018.

(Member)

Signature

Name **Dr. Abdul Hadi Al-Janabi**

Title Professor

Address Institute of Laser for Postgraduate Studies / University of Baghdad

Date / /2018.

(Supervisor)

Approval by the Deanship of Institute of Laser for Postgraduate Studies, University of Baghdad.

Signature:

Name: **Dr. Abdul Hadi Al- Janabi**

Title: Professor

Address: Dean of the Institute of Laser for Postgraduate Studies / University of Baghdad.

Date: / /2018.

الإهــداء . . . .

الى من بذل الغالي والنفيس ...

الى من كان قدوتي في الحياة ...

الى من اثرنا على نفسه .. والدي الغالي.

الى ملاذي الامن .. ودعائي الوافر ...

الى داعمي القوي .. والدتي الغالية.

الى من حملت الصبر وازاحت الهموم...

الى من لم تزغ عن جانبي ... زوجتي العزيزة.

الى سندي في الصعاب .. اخواني واختي .

الى جائزتي في الحياة .. اولادي فاطمة ومحمد .

الى من زرع الدرب ورداً بدل الشوك..

الى من انار ضوء ساطع في طريقي .. مشرفي العزيز.

الى كل من اجدني مديّنتا لهم عندما أقلب دفاتر عقلي وروحي.اساتذتي ، أهلي وأصدقائي

الى من يستحق بجدارة تعبي وسهري ودمي ... وطني الغالي .

ACKNOWLEDGEMENTS

ABSTRACT

Interferometers are widely used for sensing applications. In this work, a simple all-fiber coreless Mach- Zehnder interferometer sensor based on mode mismatch splicing method has been fabricated and demonstrated for refractive index/concentration sensing. The effect of the length and the diameter of the coreless fiber (CF) have been investigated as effective parameters for enhancing the sensitivity of the sensor. The fabrication of the sensor involves cleaving and splicing Coreless Fiber (CF) with two segments of Single Mode Fibers (SMF Corning-28). In this Singlemode-Coreless-Singlemode (SCS) structure, the CF segment acts as a sensing segment. The broadband source was connected to the SCS end while the SCS another end was connected to the optical spectrum analyzer to monitor change in the spectrum. Sucrose solution with different concentrations was prepared from (10-60) %. Three different lengths of CF (2, 4, and 6 cm) were used to perform the experiments. The diameter of CF was at 125 μm. It is found that the sensor's sensitivity has no noticeable change in sensitivity with those lengths when diameter kept fixed at 125 μm. Etching with HF 40% has been carried out to reduce the CF diameter. It is found that the sensor's sensitivity was enhanced by reducing the CF diameter by etching using HF 40% for 40 min. The maximum obtained sensitivity was 340.89 nm/RIU at materials with different refractive indices for different fluids when diameter reduced to 60 μm.

The maximum obtained sensitivity was 0.52 nm/% (corresponds to a resolution of 0.038% at a wavelength resolution of the optical spectrum analyzer of 0.02 nm) when the concentration range of sucrose solution

varied from 0 to 60%   at diameter and length of the CF of 60 μm and 2 cm respectively.

The investigating of both, fundamental mode, and High order mode at CF have been studied theoretically using Multiphysics COMSOL package by reducing the diameter of CF at (125,100,80, and 60) μm. It is found that when the diameter of CF was reduced, the fundamental mode and the high order modes confinements was more effective.

TABLE OF CONTENTS

LIST OF TABALS

LIST OF FIGURES

LIST OF SYMBOLS AND ABBREVIATONS

SMF	Singlemode fiber
MMF	Multimode fiber
PMF	Polarized maintain fiber
PCF	Photonic crystal fiber
FBG	Fiber Bragg grating
CF	Coreless fiber
MZI	Mach-Zehnder interferometer
RI	Refractive index
LP	Linear polarized
PC	Polarization controller
OC	Optical coupler
L	Cavity length
MMI	Multimode interference
n_1	Core refractive index
n_2	Cladding refractive index
V	The normalized frequency parameter or V–parameter.
K, K_0	wavenumber
λ	wavelength of light
Δ	Fractional index difference
M	Total mode number
b	normalized propagation constant
β	propagation constant
n^-	Mode index
η	Lattice pitch
I_{Tot}	Total intensity
I_1	Core mode intensity
I_2	Cladding mode intensity
$\Delta\theta$	phase difference
θ_1	Phase of core mode intensity
θ_2	Phase of cladding mode intensity
L_{MZI}	Length of Mach-Zehnder interferometer

Δn_{eff}	Effective index difference between core and cladding modes.
m	Integer number
n_{eff}^{core}	Effective index of core
$n_{eff}^{cladding}$	Effective index of cladding
$\Delta \lambda$	wavelength spacing between adjacent constructive peaks
FSR	Free spectral range
SMS	Singlemode-Multimode-singlemode fiber structure
SCS	Singlemode-Coreless-singlemode fiber structure
L_{CF}	Coreless fiber length
p	Self-imaging number
L_{π}	Beat length
λ_0	Peak spectral response
D_{CF}	Coreless fiber diameter
n_{CF}	Effective refractive index at coreless fiber section
HE	Higher order
λ_B	Bragg wavelength
Λ	Period8 of grating
MFD	Mode field diameter
B.B.S	Broadband source
OSA	Optical spectrum analyzer
RIU	Refractive index unit

Chapter One

Introduction and basic concepts

Chapter one

1.1 introduction

Recently, fiber based sensors are attracting a lot of interest due to their potential applications in communication, industry, medicine, and military applications [1-4]. Many kinds of optical fiber sensors have been designed and developed to measure various parameters such as, refractive index, humidity, temperature, magnetic fields, strain, rotation, vibration, pressure, acoustics, acceleration, etc. [5-8]. Optical fiber sensors have become more and more important; they gradually become indispensable in

Different structures have been fabricated using singlemode fiber (SMF), multimode fiber (MMF), polarization maintain fiber (PMF), photonic crystal fiber (PCF), fiber Bragg grating (FBG), and coreless fiber (CF). The field of optical fiber since the first demonstration by the Nobel laureate C. Kao [9] has become more interesting. Fabrication and enhancement continued. More researches have been done to enhancement optical fiber for many applications. In recent years several new classes of fiber were investigated. The appearance of photonic crystal fibers (PCFs) by Philip St. J. Russell in 1996 [10] was a breakthrough in fiber optic technology given these fibers not only unprecedented properties as they could overcome many limitations intrinsic to standard optical fibers

Optical Fibers have many attractive advantages and disadvantages, the advantages include their low cost of some types, small size, electromagnetic immunity and very high sensitivity. While some of its disadvantages are high cost of other types, carefully handling and unfamiliarity to the end user. But its attractive advantages show the potential of the fiber optic.

Optical fibers are the main fabrication components for optical waveguide fiber, optical filters, optical sensor, interferometers, couplers

and circulators [11-15]. In optical fiber sensor, the interference represented the main principle to measure sensitivity. There are many types of optical fiber interferometers such as Sagnac interferometer, modal interferometer, Michelson interferometer, Moiré interferometer, Fabry-Perot interferometer, and Mach-Zehnder interferometer (MZI) [16-20]. Different structure for these interferometers can be implanted. Among them, all-fiber MZI sensor has many attractive features such as broad wavelength operation range, low insertion loss, compact and robustness. All-fiber MZI can be implemented in different ways and different types of fibers, e.g., coreless fiber, photonic crystal fiber (PCF), nanofiber, polarization maintain fiber (PM), Bragg fiber, and multimode fiber (MMF) [21-26]. MZI based on CF is extensively investigated by many authors but still the most promising sensing schemes due to its unique advantages of very ease of fabrication, low development cost and very high sensitivity [27].

The principles of all the aforementioned interferometers relies on the interference phenomena. By monitoring the shift of the peak (or dip) position of spectrum, the RI of the surrounding medium could be estimated. The sensing sensitivity is the key factor to access the performance of sensing system, high sensitivity is always desired.

Design and fabrication of the refractive index (RI) / concentration (%) sensor based on multimode interference (MMI). The sensor is respond to the change in concentration for sucrose solution. Sucrose is a natural product extracted from sugar beet or sugarcane which playing an important role in human health and his nutrition which it is popular used as a raw materials in different food industries [28]. Documentation of sucrose concentration index is very important on paper-marking, food industry, chemical, and sugar production process [29]. Therefore, developing more efficient liquid concentration measurement techniques to improve the

production control and the qualities of products is very important [30]. Fiber based sensors seems more relevant for this purpose.

1.2 Optical Fiber

The principle of operation of the conventional fiber relies on total internal reflection inside a high index core surrounded by a low index cladding. The optical fiber is a cylindrical dielectric waveguide made of materials such as silica glass with slightly different in refractive index between the core where the light is guided and the cladding. The light propagation in optical fiber is extremely depends on the type of material and propagation mechanism. There are several types of optical fibers depending on waveguide mode or structure of the fiber:

1.2.1 Singlemode fiber:

Fiber with small core diameter (**a**) of about (8-10) µm allows single mode to be guided through it with clad diameter (**d**) of about 125 µm as shown in Figure 1.1(a). This type of fiber consists of doped silica core with refractive index (n_1) and fused silica cladding with refractive index (n_2) where $n_1 > n_2$ [31]. A parameter playing an important role is the cut-off condition which defined by V number or Normalized frequency as follows:

$$V = k_0 a \, (n_1^2 - n_2^2)^{1/2} = 2\pi / \lambda \, a n_1 \, (2\triangle)^{1/2} \ldots\ldots\ldots\ldots (1.1)$$

where k_0: wavenumber and define as follows:

$$k_0 = 2\pi / \lambda \ldots\ldots\ldots\ldots\ldots\ldots\ldots\ldots\ldots\ldots (1.2)$$

λ: is the operated wavelength,

$\triangle$: fractional index difference and defined as follows:

$$\triangle = n_1\text{-}n_2/\ n_1 \dots\dots\dots\dots\dots\dots\dots\dots\dots\dots\ (1.3)$$

For singlemode operation should be $V < 2.405$ for singlemode operation. The total mode number (M) can be calculated using following equation:

$$M= V^2/2 \dots\dots\dots\dots\dots\dots\dots\dots\dots\dots\ (1.4)$$

The normalized propagation constant (**b**) defined as follows:

$$b= [(\beta/k_0)^2\text{-} n_2^2]\ /\ [n_1^2\text{-}n_2^2] = [\bar{n}\text{-}n_2^2]\ /\ [n_1^2\text{-}n_2^2] \dots\dots\dots\ (1.5)$$

where β propagation constant, and $\bar{n}$: mode index Figure (1.2) shows the relation between normalized propagation constant and normalized frequency.

1.2.2 Multimode fiber:

Fiber with large core diameter of about 50-60 µm allows to multi-mode to be guided through it with clad diameter of about 125 µm as shown in Figure 1.1(b). These multimode fibers (MMF) also have two different sub-division depending on change in refractive index of the core [31]:

i- **Step index multimode fiber**: in this type of multimode fiber the refractive index of core (n_1) is greater than cladding refractive index (n_2) by one step [32]. The light rays propagate in zig-zag manner inside the core as meridional rays.

ii- **Graded-index multimode fiber**: in this multimode fiber the refractive index of core (n_1) is highly refractive index at the center and decreased gradually changing up to (n_2) [32]. The light rays propagate in the helical or skew form. (Figure 1.3).
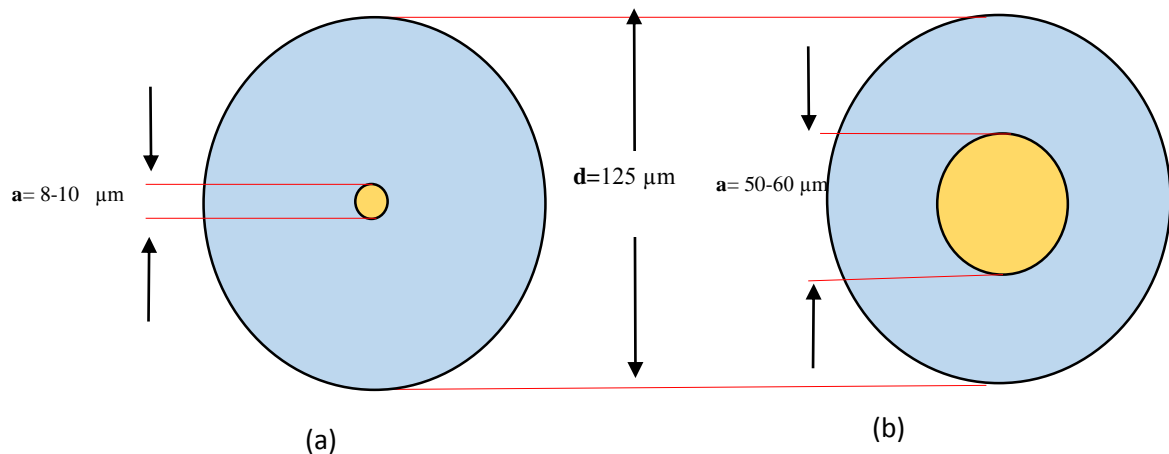
Figure 1.1. (a) Schematic of singlemode fiber, (b) Schematic of Multimode fiber [32].
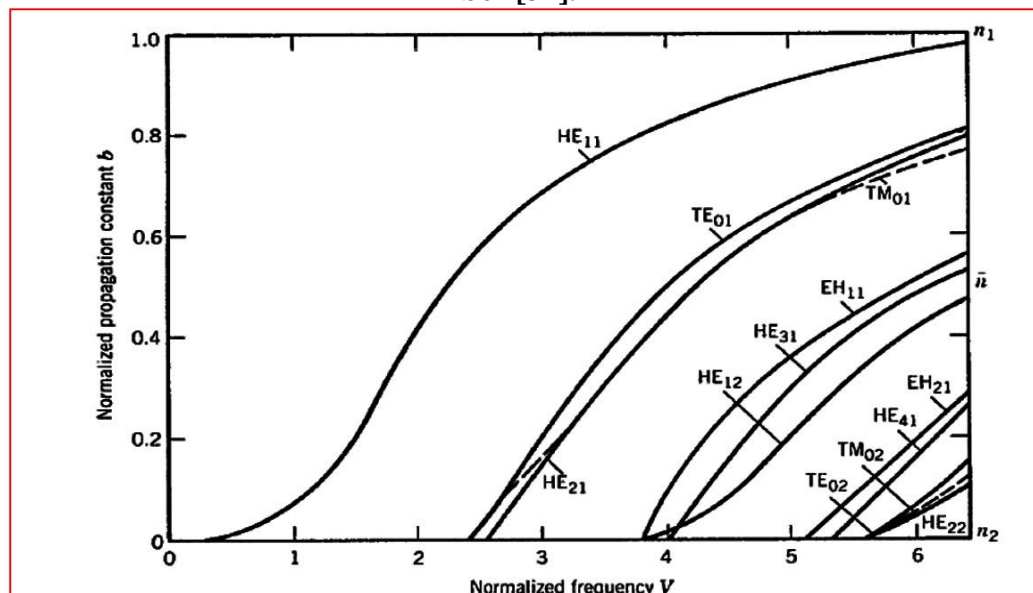
Figure 1.2. Normalized propagation constant b as a function of normalized frequency V for a few low-order fiber modes. The right scale shows the mode index n⁻. [32]
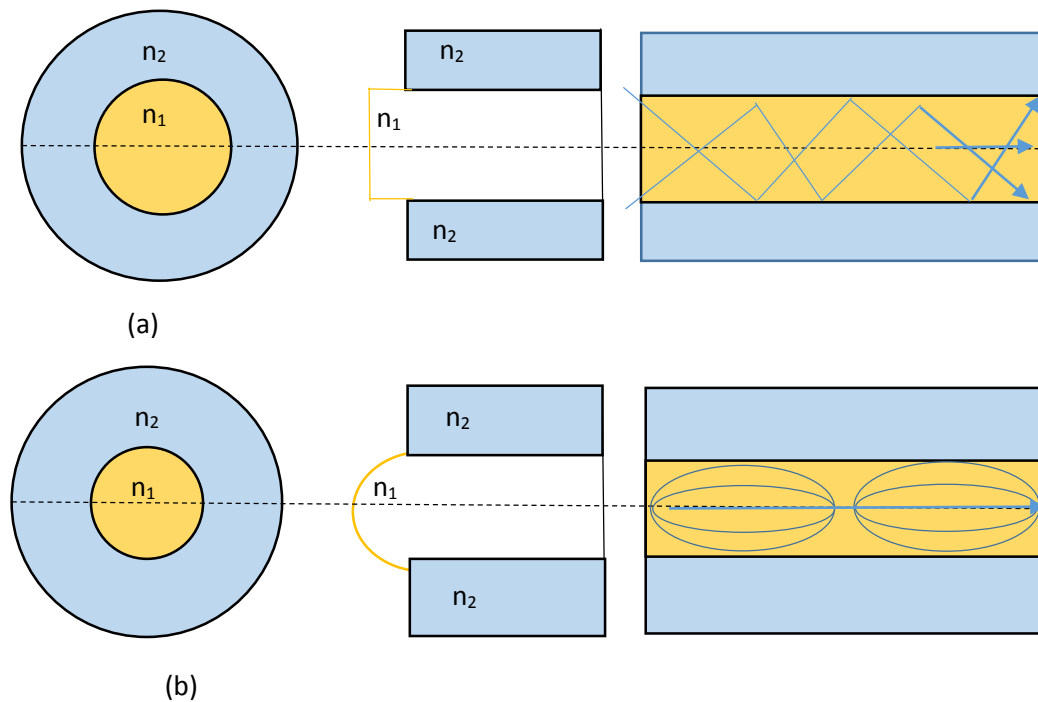
Figure 1.3. (a) Schematic of Step-index MM fiber, (b) Schematic of Graded-index Multimode fiber [32]

1.2.3 Polarization maintain fiber:

A special type of single mode fiber designed to transmit only one polarization of the input light named polarization maintaining fiber (PMF) with highly birefringence with predetermined slow and fast axes while conventional singlemode fibers are designed to carry randomly polarized light [33]. PM fibers have subdivision depending on the design used to create birefringence into:

i-   **PM Panda:** in which design two stress applying part to create symmetric birefringence to maintain the polarization of lunched light Figure 1.4(**a**).

ii-   **PM Elliptical-clad:** in which born glass silica in elliptical shape around the fiber core to create asymmetric stress, these stress on the core leads to create birefringence, Figure 1.4 (**b**).

iii-   **PM Bow-tie:** in which two opposing wings designed to create more birefringence than any other stressed design Figure 1.4 (**c**).
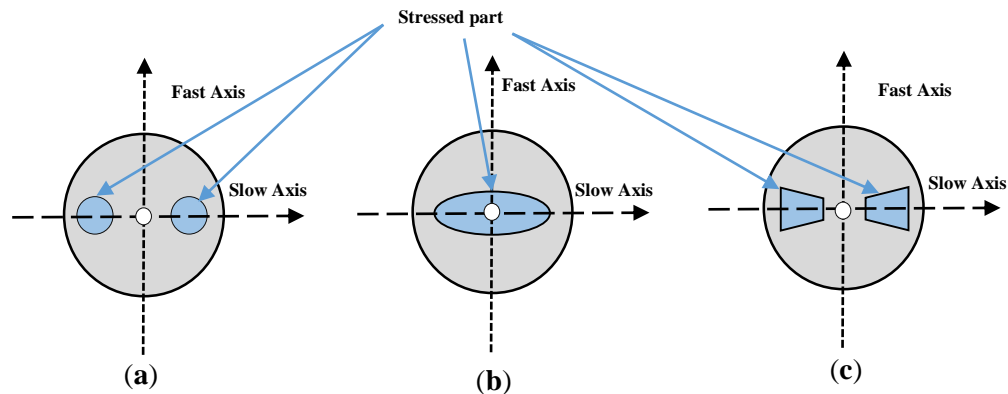
Figure 1.4 (a) Schematic of PM Panda fiber, (b) Schematic of PM Elliptical-clad fiber, (c) Schematic of PM Bow-tie fiber [33].

1.2.4 Photonic crystal fiber:

Photonic crystal fibers (PCFs), which are also called microstructured optical fibers or holey fiber. Its design with arrangement of capillaries in hexagonal arrangement filled with air. The design of this type of fibers depend on different multiple parameters like lattice pitch (η), air hole shape and diameter (**d**), diameter of core (*a*) refractive index of the glass, and type of lattice [34]. The photonic crystal fibers can be divided into two classes based on the light guiding mechanism [35]:

i- **Solid core (index-guiding fibers):** This type of PCF has a solid core. Because the refractive index of the pure silica core is larger than the average index of the cladding which is made of pure silica and air holes, light is guided in a higher index core (solid core) by modified total internal reflection from a low effective index cladding, similar

to conventional fibers [36]. The schematic of a common solid -core PCF is shown in Figure 1.5 (**a**).

ii- **Hollow core (bandgap-guiding fibers):** Hollow core fibers consists of a hollow core surrounded by micro structured cladding with a periodic arrangement of air-holes in glass as shown in Figure 1.5(**b**). In this case total internal reflection conditions are not fulfilled since the air core has a lower refractive index than the cladding. Light can propagate along the fiber only with photonic bandgap mechanism [37].

(**a**)   (**b**)
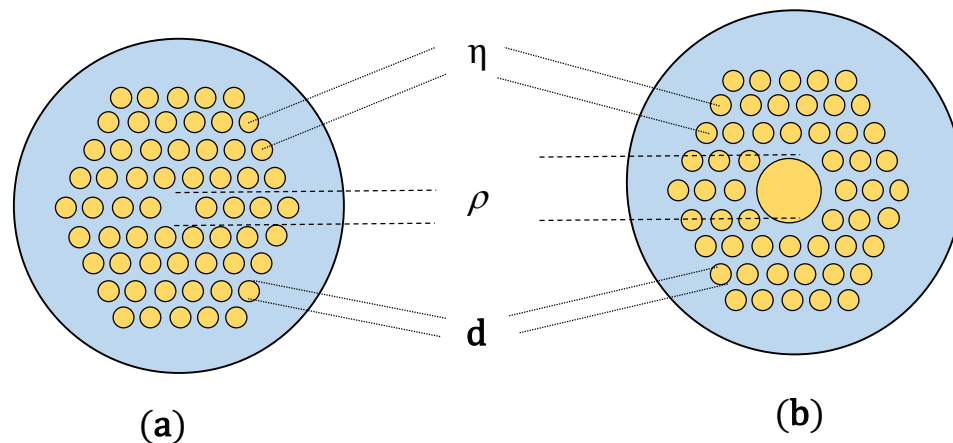
Figure 1.5.(a) Schematic of Solid core PCF, (b) Schematic of Hollow core PCF [36]

1.2.5 Coreless Fiber:

A new kind of commercialized special fiber which is drawn from a preform with a uniform RI, usually fused silica named coreless fiber (CF) where it has only cladding with diameter (**d**) 125 µm which equal to outer diameter of conventional fibers [38]. Many companies such as Thorlabs, nLight, and OFS A Furukawa company fabricate CF with different operation temperature range (-65-+300 Cᵒ), also different outer diameter

ranged (125-480) μm and wide wavelengths operation range (400-2400) nm for many applications.

The air or another surrounding refractive index medium which is lower than CF refractive index could act as multimode waveguide based on total internal reflection and multimode interference principle [29]. Figure 1.6 shows comparison between the SMF and the CF schematic.
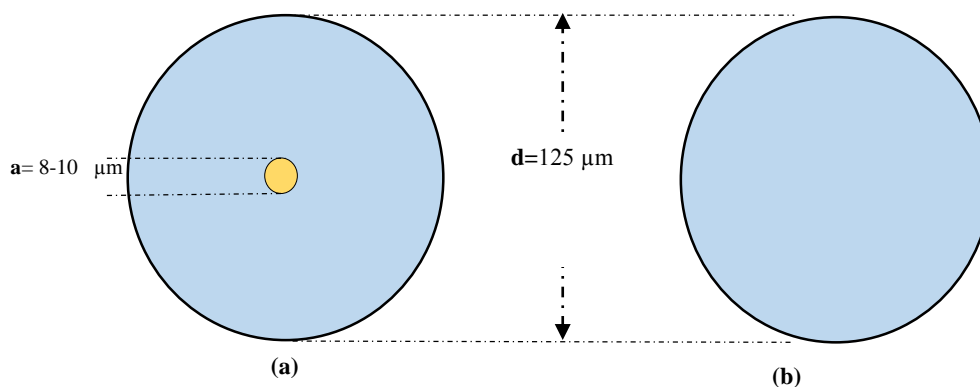
Figure 1.6 (a) Schematic of singlemode fiber, (b) Schematic of Coreless fiber [38]

Coreless fiber is considered as a special case of multimode fiber which outer diameter allows to multimode to be guided through it when the surrounding medium has lower refractive index than CF refractive index [39].

1.3 Optical fiber Interferometers

An optical Interferometers provide attractive interest in metrology applications, also offers some advantages such as stability, compactness, and rigid construction interferometers system. Two approaches are used to carry out optical fiber interferometers. First, consists of splitting and recombining two monochromatic optical beams that propagate in different

fibers. These two-arm interferometers typically require several meters of optical fibers and one or two couplers .The second approach consists of exploiting the relative phase displacement between two modes, typically the first two linear polarized (LP) modes like the LP_{01} and LP_{11}. Such interferometers based on approaches above are known as modal interferometers [40]. There are different configurations have been achieved the optical interferometers using optical fibers such as:

1.3.1 Sagnac fiber interferometer

An optical Sagnac interferometer made by splicing a piece of long conventional SMF fiber to fiber coupler with two output port to form a loop in which light is split into two beams and propagate in opposite different directions inside the same waveguide in a fiber loop [41]. The opposing signals are recombined by the coupler. A polarization controller (PC) is used at the beginning of the sensing region to adjust the polarization [42]. The path of the lunched beam is modified resulting in a phase shift and a different interference pattern because of the effect of environmental parameters in the sensing region.

If 3-dB fiber coupler is used any input power totally reflect and Sagnac acts as reflector mirror or as nonlinear mirror. Figure 1.7 shows the schematic design of Sagnac interferometer.
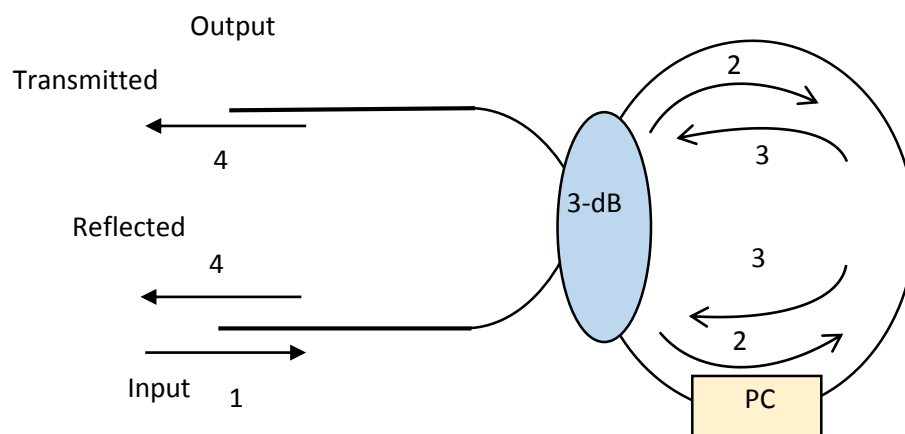
Figure 1.7. Schematic of Sagnac fiber interferometer [43].

1.3.2 Michelson fiber interferometer

This type of optical interferometer made by splicing piece of optical fiber to input (**N×N**) optical fiber coupler, the launched beam will split to two different optical path and reflect at the end of fiber by FBG or other optical reflector. The beam reflected by mirrors recombined by optical coupler (OC) to create the interference pattern at the output end [15]. Michelson in optical fiber acts as nonlinear mirror like Sagnac interferometer. Figure 1.8 shows the schematic of Michelson interferometer.
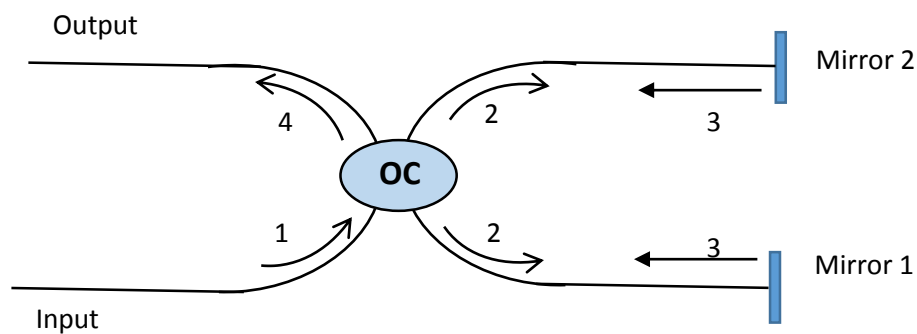
Figure 1.8. Schematic of Michelson fiber interferometer [44].

1.3.3 Moiré fiber interferometer

This type of optical interferometer based on the Moiré fringe pattern when two or more gratings lie contact at small angle θ to form the Moiré fringes. By suitable arrangement of two or three optical fibers, Moiré fringe pattern could be designed basing on the generation of interference grid pattern. Three PMF optical fibers connected to 1×3 optical fiber coupler at the input port and at the output port inserted into a glass tube and glued with epoxy [45]. Figure 1.9 shows the schematic of Moiré interferometer.
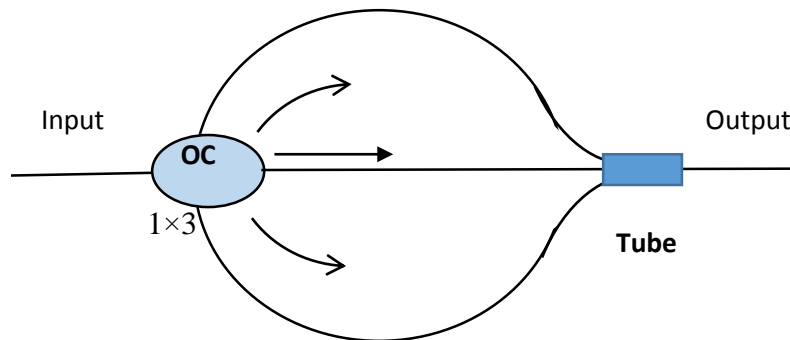
Figure 1.9. Schematic of Moiré fiber interferometer [45].

1.3.4 Fabry-Perot fiber interferometer

This type of optical interferometer consist of two optical parallel reflector based on Fabry-Perot effect, with a cavity of length L between those reflectors [28]. Reflectors can be interface of two dielectrics mirrors, or two fiber Bragg gratings, or two internal mirror achieved by splicing of polished fibers, or by coating cleaved end of the optical fiber [46]. Figure 1.10 shows the schematic of Fabry-Perot interferometer.
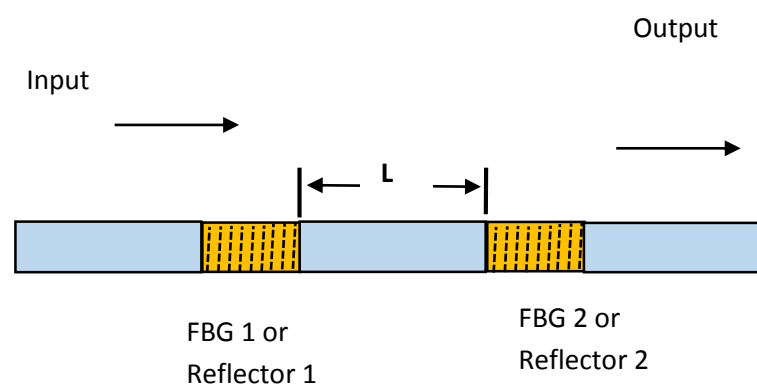
Figure 1.10. Schematic of Fabry-Perot fiber interferometer [46].

1.3.5 Mach-Zehnder interferometer

Mach-Zehnder interferometers (MZI) has attracted a lot of interest for various sensing applications due to their flexible structure, easy to fabricate, capability of responding to a surrounding variety and low cost [47]. All optical MZI by constructed in two methods, first method by using two outer couplers connected in series with two fibers. The first coupler splits the input signal into two arms, reference arm and sensing arm, another fiber coupler is used to recombine the signal. The recombined light has the interference component according to the Optical Path Difference between the two arms [48, 49]. Figure 1.11 shows schematic of MZI using outer couplers.

Reference arm

Input

OC

OC

Output

Sensing arm
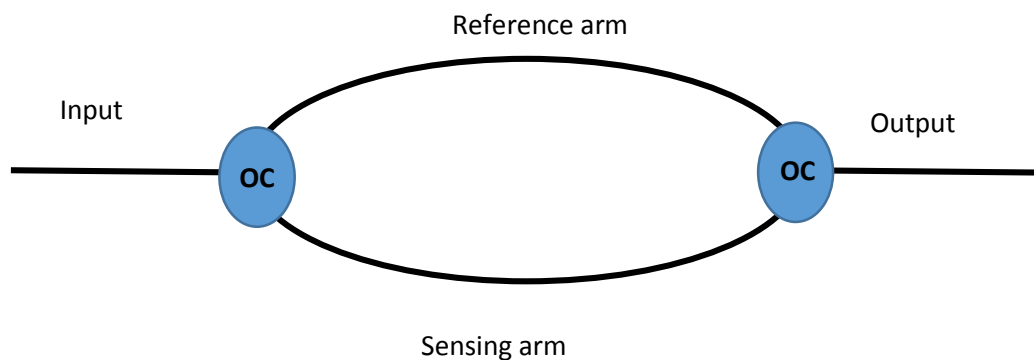
Figure 1.11. Schematic of MZI fiber interferometer with outer couplers [49].

The second method achieved by one optical fiber using splicing technique and it has same principle. In such method splicing region between two similar or different fibers acts as inner coupler [14]. In splicing region the refractive indices of both core and cladding of identical or hybrid fibers fused resulting a new area with attributed variation in refractive index. There are two splicing region, first region act as a beam splitter coupler where the entry beam will split into two beams, reference

beam and sensing beam [18]. The fundamental modes guided through the core acts as reference beam and high exited order modes which guided through cladding can acts sensing beam since it influence with surrounding environment variation. While the second splicing region acts as combiner coupler and the two beam will recombined. The two beam has interference and can be expressed by:

$$I_{Tot} = I_1 + I_2 + 2\sqrt{I_1 I_2}COS(\theta_1 - \theta_2) \dots\dots\dots\dots\dots\dots (1.6)$$

Here, I_1 and I_2 are the light intensities of core mode and cladding mode at the end of the MZI.

$\Delta\theta = (\theta_1 - \theta_2)$ is the optical path difference between the core mode and the cladding mode and can be expressed as:

$$\Delta\theta = k\Delta n_{eff}L_{MZI} = \frac{2\pi}{\lambda}\Delta n_{eff}L_{MZI} \dots\dots\dots\dots\dots\dots\dots\dots (1.7)$$

where, L_{MZI} is the physical length of MZI is, $\Delta n_{eff} = n_{eff}^{core} - n_{eff}^{clad}$ is the difference between the effective refractive indices of the core and cladding. Equation (1.7) plays a very important role to determine whether the interference pattern is constrictive or destructive. When $\Delta\theta$ satisfies $\Delta\theta = 2m\pi$, where $m = 0, \pm1, \pm2 \dots$ is a constrictive interference. While, if $\Delta\theta = (2m - 1)\pi$, where $m = 0, \pm1, \pm2 \dots$ is a destructive interference.

If the optical path difference between the core mode and the cladding mode varies continuously, it will result in interference pattern and the measured intensity will change from a maximum $I_{max} = I_1 + I_2 + 2\sqrt{I_1 I_2}$, (if $\Delta\theta = 0$) to a minimum of $(I_{min} = I_1 + I_2 - 2\sqrt{I_1 I_2})$. Therefore, the fringe visibility constant or fringe modulation depth can be defined as:

$$\frac{I_{max} - I_{min}}{I_{max} + I_{min}} = \frac{2\sqrt{I_1 I_2}}{I_1 + I_2} \dots\dots\dots\dots\dots\dots\dots\dots\dots (1.8)$$

The spacing $\Delta\lambda$ between adjacent constructive peaks (or the free spectral range FSR) can be described as [50, 51]:

$$\Delta\lambda = \frac{\lambda^2}{\Delta n_{eff} L_{MZI}} \quad \dots\dots\dots\dots\dots\dots\dots\dots\dots\dots\dots\dots\dots\dots (1.9)$$

There are various configuration of MZI in the second method such as singlemode-multimode-singlemode (SMS) MZI, mismatch core MZI, transition PCF MZI, reflection MZI, Tapered Fiber MZI, and CF MZI as shown in Figure 1.12.

(a)

(b)

(c)

(d)

(e)

(f)
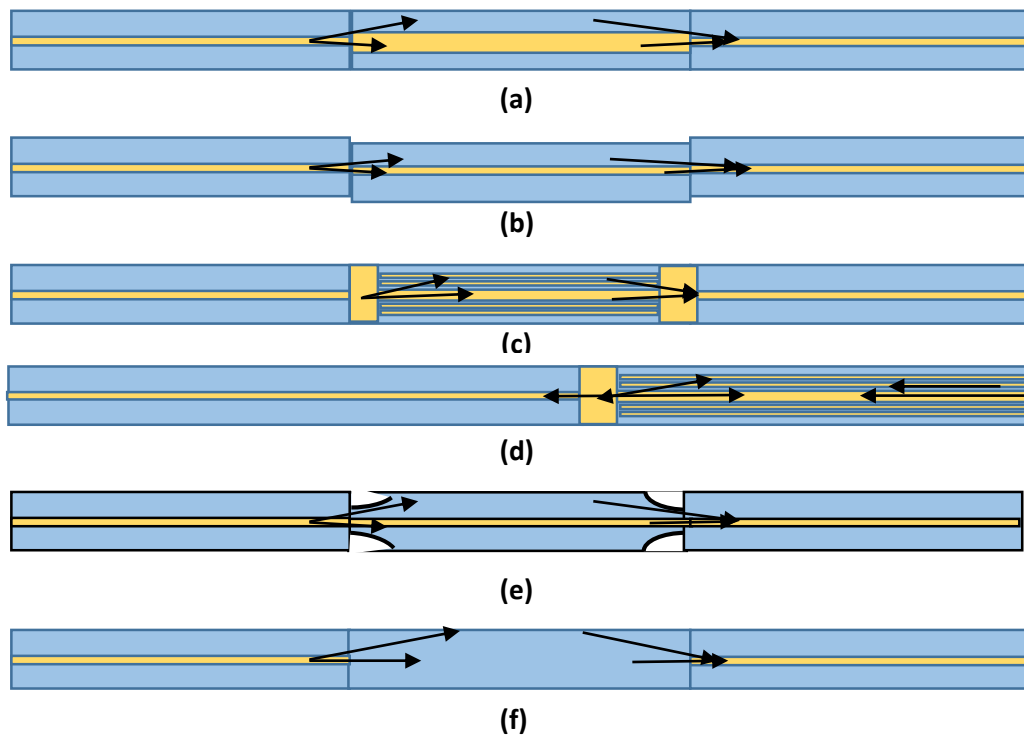
Figure 1.12. Schematic of inline MZI fiber interferometer with inner couplers.

(a) SMF-MMF-SMF, (b) mismatch core, (c) SMF-PCF-SMF transmission,

(d) SMF-PCF reflection, (e) Fiber Tapering, (f) SMF-CF-SMF [49, 52]

All types above depending on the extremely interference principle and can be expressed by equations 1.3-1.8. In the present work will be attend to fabricate CF-MZI. This structure of interferometer can formed by fusion splicing two segments of standard SMF to the two end of coreless fiber (Figure 1.11 (f)). The discrimination of modes here, based on multi-

mode interference (MMI) effect in single mode-coreless-single mode (SCS) fiber structure. As CF explained in section 1.2.6 considered a special type of MMF, multi-mode be guided through it.

According to the modes involved in the interference it can be divided into two categories. One is the interference between fundamental core mode and higher order core modes (core–core intermodal interference), another is the interference between fundamental core mode and cladding modes (core–clad intermodal interference). Depending on self-imaging effect the MMI can be occur between modes [53]. The self-imaging (also named lensless imaging) means that an input field distribution repeats itself in periodic repetition in a certain distance without any helped device between object and image [54]. The mode-mismatch between SMF and CF allows the fundamental mode in SMF to couple into a CF. Then, the fundamental mode begins to diffract within the CF. High order modes are excited and propagated independently along the CF section. These high order modes are interfered with each other and appeared as a superposition of their mode field. Generally these high order modes produce a complicated field distribution due to multimode interferences (MMI) effect. Nevertheless, reproducible bright images or what is called self-imaging of the input field can be created at certain positions where the excited modes are in phase [55]. The length and the diameter of the CF are key parameters in the design of such sensor. According to MMI theory, the length of the CF can be given by [2, 9, 12 and 14]:

$$L_{CF} = p \left(\frac{3L_\pi}{4} \right) \qquad \text{with p=0, 1, 2, } \dots\dots\dots\dots\dots\dots\dots\dots \text{ (1.9)}$$

Where the parameter p denotes the constructive interference number (self-imaging number). Such constructive interference can occur at periodic intervals defined by p (p =0, 1, 2 …), at these lengths the formed

images show a profile of a narrow width and a high amplitude, and $L\pi$ is the beat length and can be expressed as

$$L_\pi = \frac{4n_{CF}D_{CF}^2}{3\lambda_0} \qquad \dots\dots\dots\dots\dots\dots\dots\dots\dots\dots\dots\dots\dots\dots\dots (1.10)$$

Thus, the peak spectral response of this CF caused by self-imaging effect can be expressed as

$$\lambda_0 = p\left(\frac{n_{CF}D_{CF}^2}{L_{CF}}\right) \qquad \dots\dots\dots\dots\dots\dots\dots\dots\dots\dots\dots\dots\dots\dots\dots (1.11)$$

Here n_{CF} and D_{CF} correspond to the effective refractive index (RI) and the diameter of CF section, respectively. Then MMI will be increase using the tapering and/or etching CF outer diameter and thus incensement in MMI due to varying in peak spectral response and sensitivity of the CF-MZI.

1.4 Optical Sensor

In recent years optical fiber sensors have played an important role in scientific research because of their advantages such as electromagnetic immunity, compact, small size, electrically isolated, wide dynamic range and low cost [12]. Essentially, optical fiber sensor operation is similar to the electrical sensor with fiber and light source instead of copper wire and electricity respectively. The high sensitivity, discrimination, response time and accuracy is most of the requirements should be present in optical fiber sensor and those playing an important role for measuring and monitoring different parameters [56]. The optical fiber sensor relies on different techniques such as:

1.4.1 Interferometric Sensor:

The most popular scheme for sensing relies on interference effect. There are many type of Interferometric sensor depending on interferometer

technique used to build such optical sensor. Fabry-Perot, Sagnac, Michelson and Mach-Zander interferometer represent a typical examples. These interferometers based on the difference between velocities of two different modes, and the relative phase displacement. Typically the design of optical fiber interferometers could be employed by the first two modes like LP_{01} and LP_{11} or the HE_{11} and HE_{21} modes [57]. Interferometric sensor have more interested research due it advantages and there many applications which mentioned in section 1.3.

1.4.2 Grating Based Sensor:

Fiber Bragg grating (FBG) is an important component in optical communication and sensors and it considered a special type of singlemode fiber in which core refractive index is modulated in periodicity (Λ) along the core length to block (or reflect) a certain wavelength [58]. Only the wavelength which has value equal to Bragg wavelength (λ_B) will reflect to the input end when broad spectrum launched where (λ_B) can be expressed in equation 1.2 [59]:

$\lambda_B = 2n_{eff}\,\Lambda$ ……………………………………….. (1.10)

Where n_{eff} is effective refractive core index and Λ is the gratin period.

There are different types of FBGs e.g. uniform FBG, chirped FBG, titled FBG and long-period FBG depending on grating parameters such as length of grating, strength of grating, and refractive index. Figure 1.13 show the schematic of FBG.
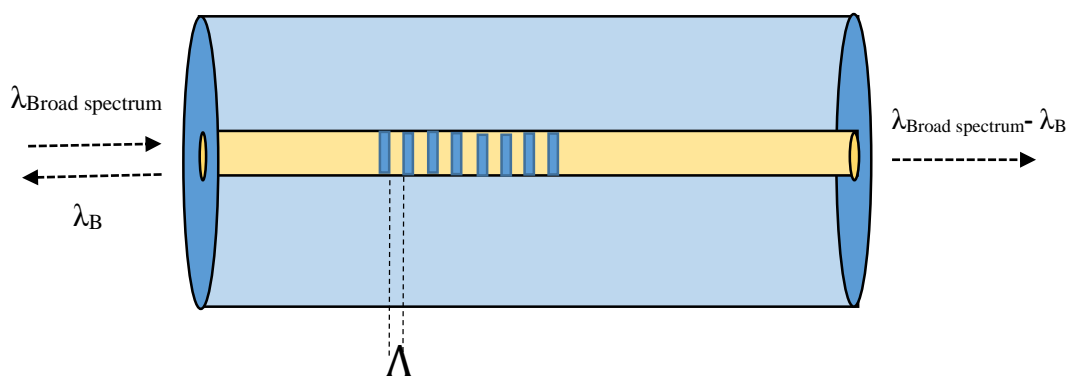
Figure 1.13. Schematic of Fiber Bragg Grating [59]

Those type of optical fiber sensor depend on different types of fiber grating used to build it. Those sensors have various applications such as temperature, pressure, strain, and dynamic magnetic field depending on Bragg diffraction principle [60]. Bragg wavelength various with any variation of such parameters. The shift in Bragg wavelength indicates the magnitude of the sensitivity to each parameter.

1.4.3 Distributed Sensor:

In such type of optical sensor the scattering principle plays an important role to measure the sensitivity such as Raman scattering, Rayleigh scattering and Brillouin scattering, where these scattering results from the interaction of photons with material characteristics features. When light beam propagates through an optical fiber, photon with specific energy will interact by stimulated or spontaneous effect such as density of material, temperature, and strain [61]. The detection result is variation in frequency, amplitude, and phase of light scattered during its travel along the optical fiber. Such types of optical fiber sensor have many applications to monitoring the change in physical parameters e.g. temperature, strain, vibration, and birefringence. Also, it could be used in the civil structural monitoring of pipelines, bridges, dams, and railroads. The mean principle of such type of optical sensor depend on physical principle of scattering, in which the optical signal entered the optical fiber will redistributed by mechanism of Raman, Rayleigh or Brillouin scattering [62]. If the physical parameters is changed, since the optical fiber provide unique spatial distributed measurement. Then the scattered signal will be modulated according to the change of those parameters and providing accuracy spatial and temporal measurement.

1.5 Optical Fiber Splicing

To fabricate fiber optical interferometers and optical sensor in previous sections, the fiber tips should be spliced to the sensing system. Various methods has been demonstrated to connect two fibers tips such as CO_2 laser, gradient index fiber lenses, a filament splicer, and Fusion splicer [63]. Fiber splicing is real challenge especially because of the small core fiber and the hybrid splicing. Arc fusion splicing of fibers is an established method for joining optical fibers tips, ensuring minimum splice loss and excellent reliability. Optical fibers with fused silica and cladding size (125 µm), protector coating and protector jacket prepared to splice [64]. The splicing equipment for these fibers is widely available. Fusion splicing process involves localized melting of two fiber tips pressed together [65], when fiber coating removed. Tension forces of surface cause glass to flow when viscosity is low enough, a joint forming with continuous structure and smooth, round external surface [66] (Figure 1.14).
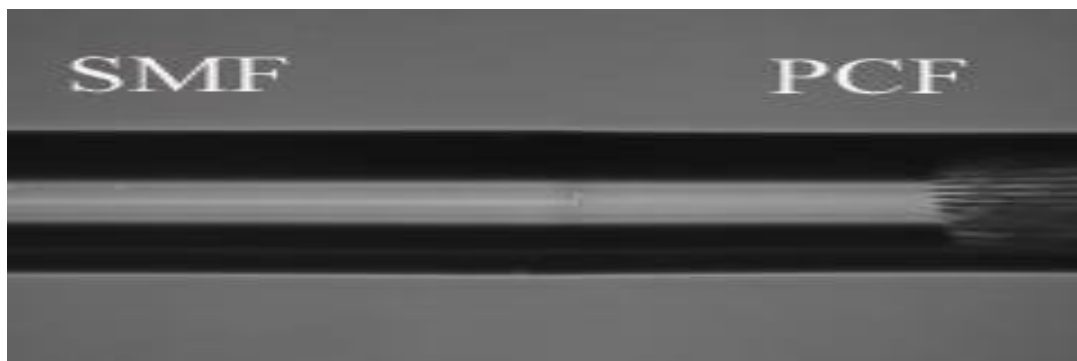
Figure 1.14. Two identical hybrid fibers (125 µm SMF to PCF) after arc fusion (In Applied photonic Fiber lab. / Institute of laser for postgraduate studies – University of Baghdad

The fiber parameters which almost affected on splice loss in single mode fiber are Mode Field Diameter (MFD – the diameter of the light-carrying

region of the fiber) and Core-Clad Concentricity. Estimated loss from mismatches in MFD can be calculated from the following equation:

Loss (dB) = 20 x Log$_{10}$ [(2 x MFD$_1$ x MFD$_2$) / (MFD$_1{}^2$ + MFD$_2{}^2$)] …….... (1.11).

The geometry of any fusion splicer is illustrated in Figure 1.15. There are many important parameters must be taken into a consideration. The first parameter called "gap" which indicate the distance between the two fiber tips before splicing. This parameter can be effective when manual mode is used in fusion splicer, also Zero gap occurs when fibers tips ends are spliced together at a position called the "touch point". Furthermore, the fiber tips pushed further together in "overlap", which indicate that fiber tips spliced together. The second parameter called "offset" which measured the distance of the touch point from the electrode axis [65].
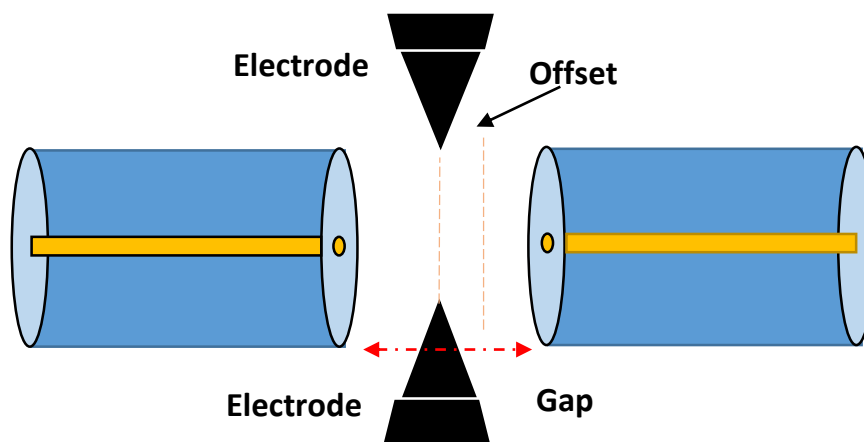
Figure 1.15. The fusion splicer geometry. Two variable parameters, gap/overlap and offset, determine the position of the fibers with respect to the electrode axis [65].

The third parameter is called "Arc power" indicate the magnitude of power impose on the two fiber tips end from both electrodes. The fourth important parameter is "Arc Time" which indicate the time of impose arc

power form electrodes. All above parameter can determine the loss in splicing process. The splicing loss can be decreased by choice optimum parameter to splicing identical or hybrid fibers. The arc fusion splicer can be used to splice different types of fiber ends together for different applications.

1.6 Optical Fiber Etching

Since the sensitivity plays an important role in optical fiber sensor, many techniques were used to enhance the sensitivity such as fiber tapering and/or etching in order to decrease the outer diameter of the fiber. Etching referred to the removal of material from a wafer surface [67].

Different approaches used to taper fiber diameter by using mechanical stretch, or fusion arc, or chemical acid. In mechanical stretch etching, when the fiber is heated to a specific high temperature, giving an extra degree of freedom to the tapering process. The heated fiber could be pulled out using two motors with certain speed to management the tapering process. While in fusion arc this process can be done using Arc fusion splicer with tapering parameters [65, 68].

There are two approaches of chemical etching. The first approach, a Wet etching in which the fiber is imposed in the chemical solution such as hydrofluoric (HF) acid [69], ethylenediamine pyrocatechol (EDP), potassium hydroxide (KOH), or tetramethylammonium hydroxide (TMAH). Multiple chemical processes involved in fiber etching to remove material from the fiber surface [70].

The second approach a Dry etching by using chemical gases flow e.g. flow of Perfluoroisobutylene (C_4F_8), or nitrogen trifluoride (NF_3), or sulfur hexafluoride (SF_6)[71, 72]. The waist size should be as small as possible, those will increase the chance of more mode interaction with surrounding refractive index medium. Generally, the interaction between

the evanescent field and the surrounding medium will be enhanced when the fiber diameter decreased. So, to make the structure more sensitive to the surrounding RI, the cladding of the fiber is usually removed by extra processing such as HF etching and/or fiber tapering of the fiber structure [73].

Furthermore, there is a trade-off between the sensitivity and the visibility of the sensor when it is applied to sense a medium of a larger absorption coefficient giving rise to a compromise between the decrease in fiber diameter and the sensor visibility [74]. When the surrounding RI around CF increases, the effective fundamental mode diameter will increased also. Therefore it needs the outer diameter to be decreased to enhance the sensitivity [75]. Using etching or/and a tapering process has an attractive advantage to reduce outer CF diameter and reduce the confinement of fundamental mode, those make it more sensitive to external perturbation [76]. By controlled etching process it could select a desired outer diameter depending on etching/time rate depending on material where fiber imposed in it or the process which used.

1.7 The Aim of the work

1. Fabrication of CF-MZI structure sensor to monitoring sucrose concentration variation**.**
2. Study the influence of the change of CF diameter on obtained sensitivity.

1.8 Literature review

All-fiber Mach Zehnder interferometers sensors have played an important role in both fundamental and applied research during the past ten years. MZI has been proposed and constructed experimentally with different optical fiber types and configurations. The survey will be focused on this approach. The most significant published work are summarized in table (1-1).

Table (1-1): Summary of the Published Works in Refractive Index Sensor.

year	Author	A brief of Published Work	Sensitivity	Reference
2007	R. Kamikawachi et al	Influence of the surrounding refractive index MZI using a cascaded long period grating (2 LPG between SMF), BBS (1450-1600)nm, RI (1.0-1.446)	−1554.1 nm/RIU	77
2008	Z. Tian et al	Single-Mode Fiber Refractive Index Sensor Based on Core-Offset Two new types of fiber-optic interferometers (Mach–Zehnder and Michelson) using core-offset attenuators, BBS (1520-1610)nm, RI (1.3-1.4)	0.333/0.01 RIU	78
2009	P. Lu et al	measurement of refractive index and temperature is proposed by using Mach–Zehnder interferometer realized on tapered single-mode optical fiber, BBS (1400-1600) nm , RI (1.3-1.36)	-23.188 nm/RIU & 0.071 nm/ °C -26.087 nm/RIU & 0.077 nm/ °C	79
2010	J. Wang et al	Mach–Zehnder interferometer (MZI) coupled microring is demonstrated experimentally to obtain a high sensitivity as well as a large range for measuring change in refractive, BBS (1520-1620) nm , RI (1.0 -1.538)	111 nm/RIU	80

2011	J. Yang et al	Taper-based Mach–Zehnder interferometer (MZI) embedded in a thinned optical fiber is demonstrated as a highly sensitive refractive index (RI) sensor by decreasing the diameter of the thinned fiber and increasing the interferometer length of the MZI, BBS (1460-1580) nm, RI (1.33-1.42).	2210.84nm/RIU	81
2011	J. Yang et al	Femtosecond laser micromachining and arc fusion splicing were used to concatenating two micro air-cavities with two SMF to proposed Highly sensitive and robust refractive index (RI) fiber sensors, BBS (1450-1600) nm, RI (1.33-1.36).	172.4 nm/ RIU	82
2012	L. Xue et al	Enhance the sensitivity of singlemode-multimode-singlemode (SMS) fiber structure in the measurement of surrounding refractive index (RI) depositing the multimode fiber section with a high RI overlay , BBS (1520-1600) nm, RI (1.31-1.35)	900 nm/ RIU 206 nm/ RIU	74
2013	L. Huang et al.	refractive-index sensor composed of a short no-core fiber (NCF) sandwiched between two pieces of single-mode fibers, BBS (1400-1600)nm ,RI (1.3-1.452)	227 nm/RIU	83
2014	C. Chen et al	The two optical coupling structures are a duplicate of the beam splitter, an optical component of the MZI interferometer	59.7 nm/RIU	84

		Using CO2 Laser Irradiation to fabricate it, this (MZI) used to test changes in the refractive index of sucrose solutions at different concentrations, BBS (1520-1600) nm, RI (1.3-1.38).		
2014	Z. Liu et al	Demonstrated the refractive index (RI) characteristics of a singlemode-claddingless-singlemode fiber structure filter based fiber ring cavity laser sensing system, Fiber laser (1555-1565), RI (1.333-1.3707).	131.64nm/RIU	85
2014	Y. Zhao et al	highly sensitive liquid concentration sensor based on a single-mode–multimode–single-mode (SMS)fiber structure cascaded with a FBG, BBS (1520-1570) nm ,RI(1.3-1.45)	286.2 nm/RIU	26
2015	H. Luo et al	measurement of refractive index (RI) and temperature based on a microfiber-based dual inline Mach–Zehnder interferometer (MZI), BBS (1510- 1590) nm, RI (1.331-1.335)	-23.67 nm/RIU & 81.2 pm/ °C 3820.23 nm/RIU & -465.7 pm/ °C	86

2015	X. Bia et al	the refractive index (RI) sensing characteristic based on the bandpass spectrum caused by the self-imaging effect in the single-mode-multimode-single-mode (SMS) fiber structure using NCF,BBS (1200-1280)nm , RI (1.334-1.434)	230 nm/RIU	87
2015	R. K. Zarzoor et al	Chemical sensor based on a solid-core photonic crystal fiber interferometer using PCF, Laser Diode 1550nm, RI (1.0-1.358)	15420 nm/mol	52
2016	Q. Wang et al.	Mach-Zehnder mode interferometric refractive index sensor, which is based on splicing points tapered SMF-PCF-SMF (SMF, single-mode fiber; PCF, photonic crystal fiber) structure with different taper diameter, BBS (1530-1550) nm, RI (1.3333-1.3737).	260 nm/RIU	88
2016	Y. Zhu et al.	The sucrose concentration measurement and characteristics of light coupling taper structure on sensitivity with various fabrication processes of taper structure for all fiber Mach–Zehnder interferometer (AFMZI) using fusion splicer with electrical discharge, BBS (1500-1600) nm , RI (1.333-1.403)	104.20 nm/RIU	30
2016	Q. Wang et al.	Refractive index sensor with high sensitivity based on Mach–Zehnder interferometer formed by cascaded two single-mode fiber tapers, ASE (1520-1570) nm, RI (1.33-1.38).	158.4 nm/RIU	89

2017	H. Dong et al	Coreless side-polished fiber structure to implement multimode interference (MMI) and high sensitive refractive index (RI) sensors, BBS (1500-1650) nm, RI (1.3-1.44).	28000 nm/RIU	90
2017	Q. Wang et al	A high sensitivity of splicing regions tapered photonic crystal fiber (PCF) Mach–Zehnder Interferometric refractive index (RI) sensor compared with cascaded bi-tapered single-mode fiber (SMF) Mach–Zehnder interferometer (MZI), ASE (1535-1565) nm, RI (1.33-1.38).	240.16 nm/RIU	91
2017	N. A. Salman et al	Photonic Crystal Fiber Interferometer Based On Refractive Index sensor for different refractive index of direct splicing and splicing points tapered SMF-PCF-SMF Mach- Zehnder interferometer, Laser Diode 1550 nm , RI (1.33-1.38)	7.4 pm /RIU	92

Chapter Two

Experimental setup and Procedures

2.1 Introduction:

Optical Fiber sensor based on multimode interference has attractive applications. Many types of interferometers have been established and investigated. MZI is one of the most promising interferometers used in sensing field for monitoring and measuring various parameters, among these parameters, refractive indices, and concentration.

In this chapter, CF-MZI structures with different lengths of CF (from Thorlabs.) were designed and fabricated to verify the characteristic that sensitive to concentration/RI using two different splicing conditions. This interferometer was fabricated by splicing a short length of (CF) between two standard SMFs. CF is used as the sensing element in MZI instead of MMF. The mode-mismatch splicing technique is employed for the implementation of the all-fiber MZI sensor.

2.2 System Layout:

The all system layout is shown in Figure (2.1). The all parts of this system, fabrication, and methods are explained next.
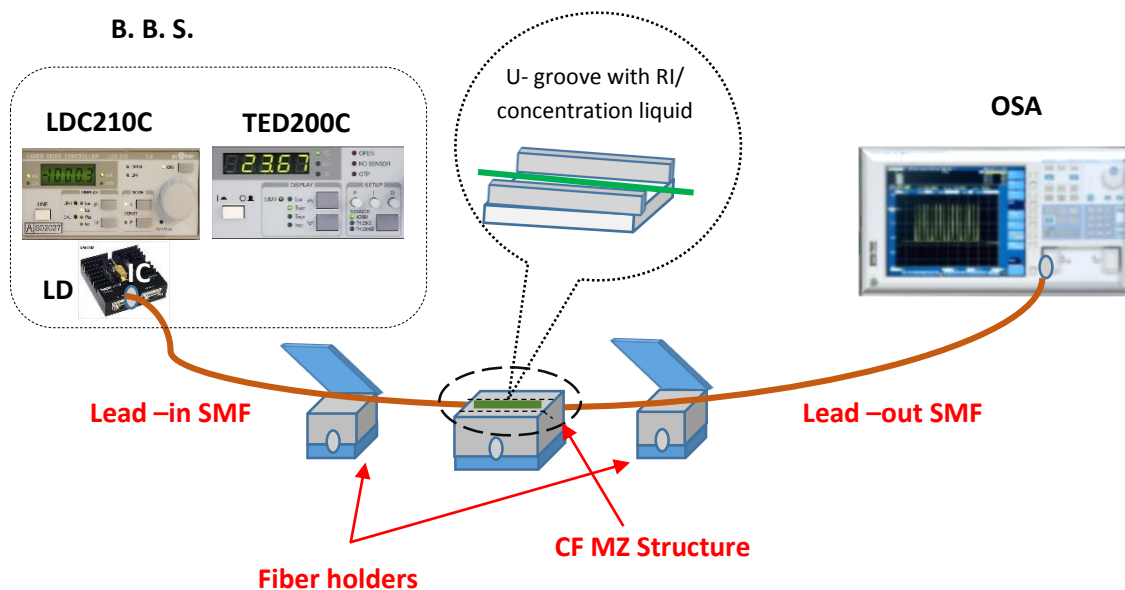
Figure 2.1. Experimental setup schematic of all-fiber CF MZI sensor

2.2.1 Broadband light source (B.B.S)

The source used in this experiment is broadband source with wavelength range (1500-1600) nm with spectral near Gaussian profile and low ripple.

The light source consists of four parts: Superluminescent laser diode (SSLD IC Chipset), Laser Mount (LM), Temperature Controller (TED200C) and Laser Diode Controller (LDC210C) (LM, TED200C and LDC210C from Thorlabs Company).

The optical signal is transmitted from IC Chipset (from COVEGA Company) where IC is consider as the main part of the SSLD. IC involves 14 pins fixed on a mount. LM14S2 Universal 14-pin Butterfly Laser Diode Mount (from Thorlabs Company) used to fix IC with top surface has heat sink fins and a recessed region to mount the laser diode.

TED is an extremely precise temperature electrical controller connected to the laser mount and it is used for a wavelength stabilization. A LDC is a device that controls values of the current. It determines the threshold where the laser signal emits. (Appendices A, B, C, and D).

2.2.2 Single-Mode Fiber (Corning SMF-28):

Single mode fiber (SMF-28) is considered the "standard" optical fiber for submarine, telephony, cable television, and private network applications in the transmission of data, voice and \ or video services.

The fiber SMF-28 is optimized to highest information-carrying capacity and lowest dispersion for use in the 1310 nm wavelength region and also in 1550 nm wavelength region can be used effectively. Corning fiber (SMF-28) has homogenous geometric properties such as high strength, and low attenuation to deliver excellent performance and high

reliability. The optical specifications of fiber Corning (SMF-28) are presented in the table (2.1)

Table (2-1): Optical specifications of Corning (SMF-28) [Appendix E].

Fiber attenuation	
Wavelength (nm)	Maximum value (dB/km)
1310	0.33-0.35
1550	0.19-0.20
1625	0.20-0.23
Mode-Field Diameter (MFD)	
Wavelength (nm)	MFD (μm).
1310	9.2 ± 0.4
1550	10.4 ± 0.5
Dispersion	
Wavelength (nm)	Dispersion value [(ps/(nm*km)]
1550	≤ 18.0
1625	≤ 22.0

2.2.3 Coreless Fiber (Thorlabs):

Coreless fiber FG125LA is the fiber used in this experiment. It consider special type of multimode fiber fabricated by Thorlabs Company could be spliced to the ends of standard fiber. Operated with wide wavelength range with return loss > 65 dB with 0.25 m coated with acrylate. CF has different refractive indices depending on operating wavelength, where it RI raise to

1.444 at wavelength 1550 nm. The optical specifications of Coreless fiber are presented in   the table (2.2) [Appendix F].

Table (2-2): Optical specifications of Coreless Fiber [Appendix F].

Coreless Fiber Specific	
Wavelength range (nm)	400-2400
Glass Diameter (µm)	125±1
Coating Diameter (µm)	250±5%
Operating Temperature C^o	-40 to 85
Glass Refractive index	1.467287 @ 436 nm 1.458965 @ 589.3 nm 1.450703 @1020 nm 1.444 @1550 nm

2.2.4 Optical Spectrum Analyzer OSA:

An Optical Spectrum Analyzer (or OSA) is a precision instrument designed to measure and display the distribution of power of an optical source over a specified wavelength span. An OSA trace displays power in the vertical scale and the wavelength in the horizontal scale.

Optical spectrum analyzer OSA (YOKOKAWA, Ando AQ6370) being used to monitor the interference spectra of the sensors. Characteristics of this device are:

- Wavelength range: 600nm to 1700nm
- High wavelength accuracy: ±0.01nm
- High wavelength resolution: 0.02nm
- Wide dynamic range: 78dB typ.
- Wide level range: +20dBm to -90dBm

- Fast measurement: 0.2 sec. (100nm span)

- Applicable to single-mode and multimode fibers

Figure (2.2) shows the image of OSA used in the experiment.
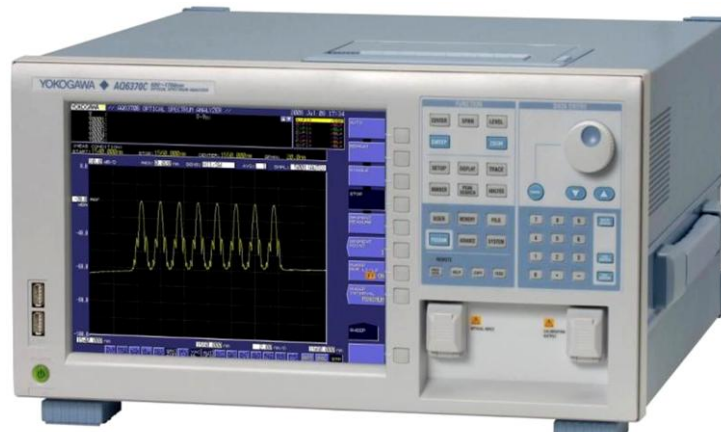
Figure (2.2): photograph of optical spectrum analyzer (OSA).

2.3 The Experimental Procedures of the Work:

Many procedures were done to fabricate CF-MZI sensor. The next subsections will explain those procedures:

2.3.1 Singlemode-Coreless fiber-Singlemode (SCS) structure:

At first, Singlemode-Coreless fiber-Singlemode structure is proposed and fabricated by splicing three different lengths of the CF between two SMFs at the same length (1.5 m) in two splicing approaches. These approaches are: auto-mode and manual-mode using Fujikura FSM-60s Fusion splicer. The procedure of the SCS structure fabrication is explained in the next sections:

2.3.1.1 Singlemode-Coreless fiber-Singlemode Fibers Cleaving:

In order to prepare optical fiber for fusion splicing, the two fibers ends should cleaved at accepted angle to minimize the splicing losses and to obtain a good splicing. The first step for cleaving fibers was done by removing the polymer coating layer using mechanical stripping or alcohol.

In this experiments, removing any protective coating such coatings can normally be mechanically removed with certain tools such as Optical Fiber Stripper (JIC – 375 Tri – Hole). The optical fiber stripper used for Stripping (by Fujikura Company).

Figure 2.3.: Optical fiber Cleaver (CT-30).

The second step to prepare the fiber was done by fiber cleavers (cleaving machines) which allow to clamp the fiber into a well-defined position, to impose a suitable amount of the tension, and to make the cleaving process by touching the fiber end with a sharp blade. The cleaving which cuts the fiber in 90º angle. The third step is the cleaning the conventional single mode fiber (SMF-28) by alcohol and tissue, figure (2.3) shows the photograph of optical fiber Cleaver (CT-30) (by Fujikura Company), which have been used in this experiment. The above steps repeated with both types of the fibers used in this experiment, the SMF, and the CF.

2.3.1.2 Coreless Fiber Etching procedures:

One of the techniques to further enhance the sensitivity of the SCS structure is by decreasing the CF diameter. The target was to reach 60 µm in diameter. This could be achieved by etching the CF with acid solution pre or post SCS structure fabrication. Then, the fabricated SCS structure was fixed in the quartz material U-shape groove (Figure 2.4). This groove was used to contain the etching solution acid (HF 40%) and to test the change in solution RI / concentration. The CF MZI is then tightly stretched and fixed by two bare fiber holders placed on 3-D (xyz) mount stage (Newport). Both ends of the U-shape groove are sealed. Three different lengths (2, 4 and 6 cm) of CF- MZI with diameter of CF at125 µm were all etched for 40 min in the hydrofluoric solution HF (~ 40%) purity (from Himedialabs Company). This resulted in a decrease of CF diameter from 125 µm to 60 µm. The purpose of fiber etching is decrease the outer diameter and to allow interaction of propagating light and surrounding RI. Figure 2.5 shows the CF diameter as a function of time.
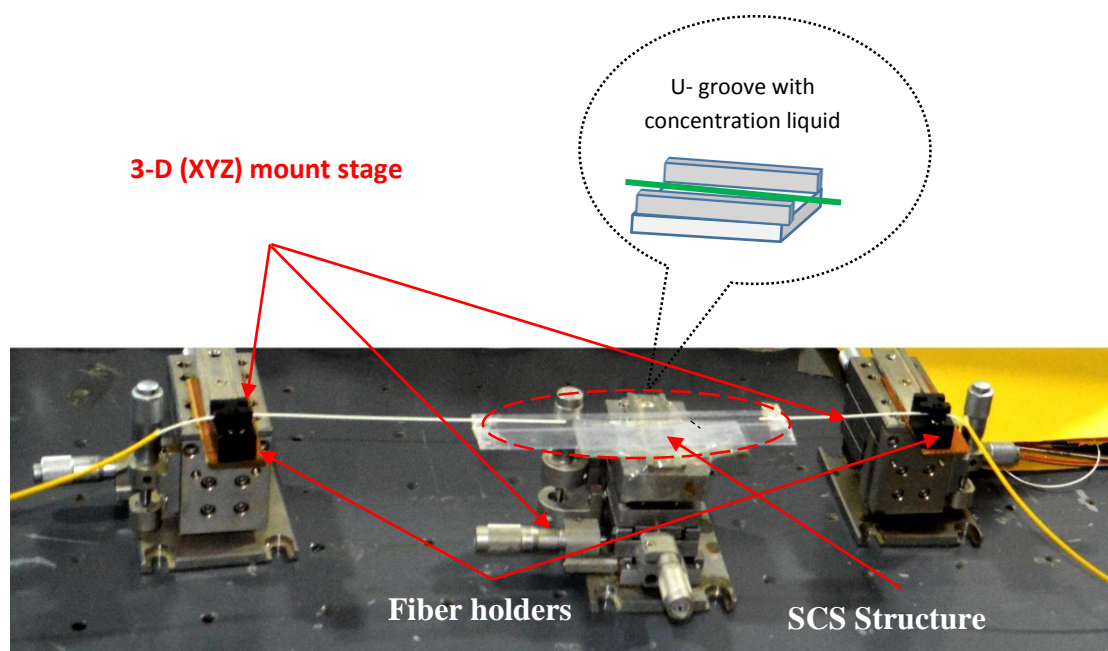
Figure 2.4. SCS etching experimental setup.
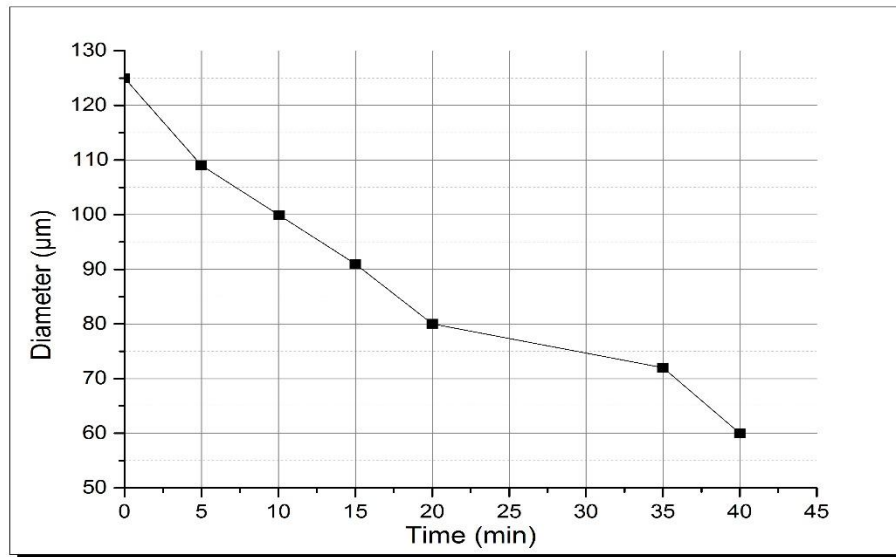
Figure 2.5. CF diameter as a function of time

Figure 2.6 represents a microscopic images of CF etching with different diameters imaged under optical microscope.
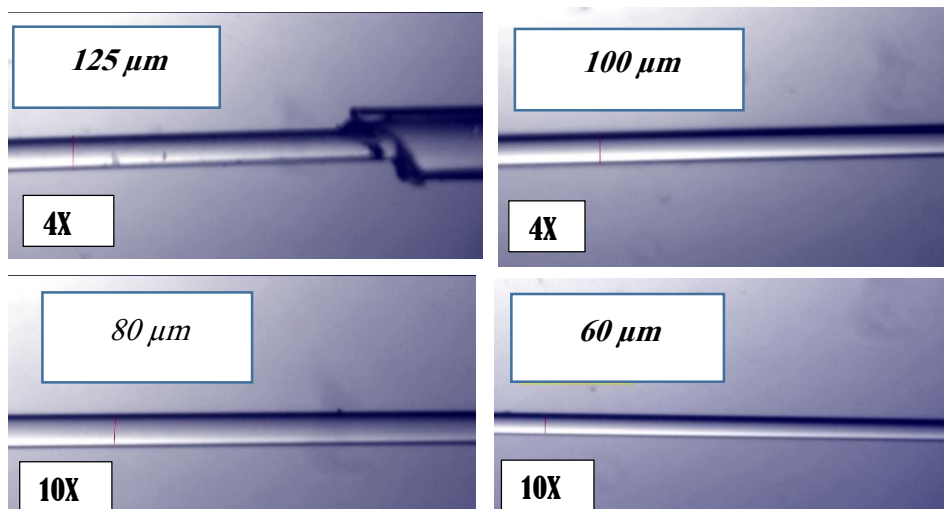
Figure 2.6. Microscopic image of CF diameter etching with time

A transmission optical microscope from (Euromex Company, Holland) was used, as shown in figure (2.7), to see top view CF diameter

after the etching This microscope has different magnification power (4 X, 10 X, 40 X and 50 X).

Figure 2.7. **The Transmission Optical Microscope**

2.3.2. Singlemode-Coreless fiber-Singlemode Fibers Splicing

The SMF (Coring SMF-28) sections have 1.451 and 1.444 refractive indices for the core and cladding, respectively. The core and the cladding diameters of the SMF sections were 9 µm and 125 µm, respectively. The CF has refractive index of 1.444 at 1550 nm and diameter of 125 µm. Therefore, the same refractive indices of 1.444 for the SMF clad and the CF reserves the optical homogeneity. The fabrications process was as follow: Firstly, CF with 125 µm diameter and 6 cm length is cleaved according to a certain length range and both ends are spliced with two standard SMFs using a fusion splicer with automatic mode to form SMF-CF-SMF (SCS) structure as shown in Figure 2.8 a.

In the second approach, the CF has been etched using HF (~40%) before splicing the CF with SMFs to reach a CF diameter of 60 µm. After etching the CF, the cleaving of fiber end face become very difficult. Consequently, bad cleaving of these etched CFs makes it not easy to auto

splice the CF and SMFs with a good repeatability and low loss. Therefore, manual splicing mode was used with repeated arc discharge technique to reduce the splicing loss as much as possible as shown in Figure 2.8 b. The fusion splicer set to the optimized splicing parameters listed in table (2-3).
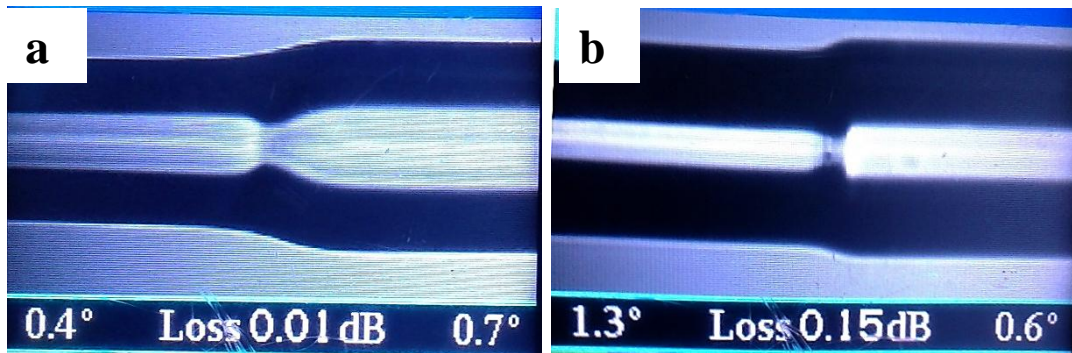
Figure 2.8. : a- The splicing region between SMF and CF using automatic splicing mode, b- The splicing region between SMF and CF using manual splicing mode.

Table (2-3) Optimized parameter of manual SMF/CF fusion splicing.

Splicer parameters	Fiber Types
	SMF/CF
Perfused power	Standard
Perfused time	180 ms
Overlap	15 µm
Gap	10 µm
Arc 1 power	STD+25 bit
Arc 1time	1000 ms

The main disadvantages of the second approach are the etched fibers become very fragile and the handling of these fibers are not easy. The two used approaches for etching did not reflect any noticeable change on measurement sensitivity. Therefore, it was used the first approach to

fabricate CF MZI. For more clarification a histogram has been drawn as follows (Figure 2.9.) to show the splicing loss for both approaches.
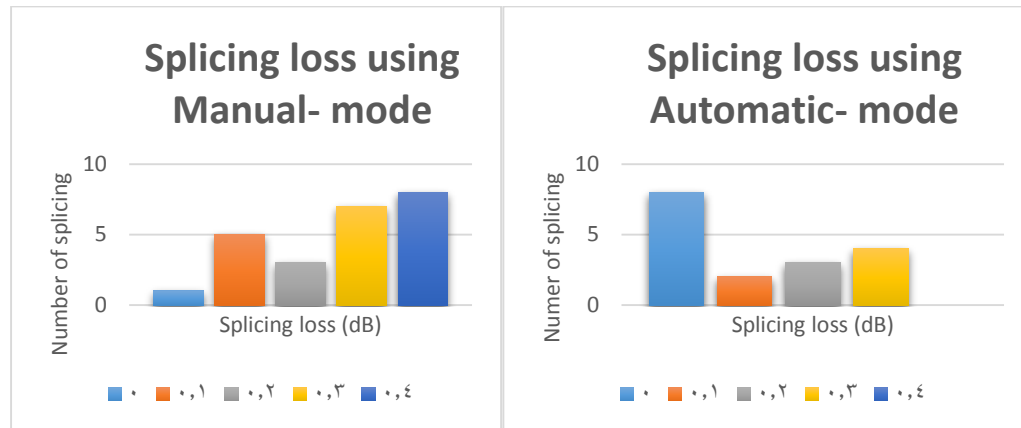
Figure 2.9. Splice loss histogram for fusion splicing between CF and SMF using Automatic splicing mode and Manual splicing Mode.

The typical steps to perform fusion splicing are:

- Remove any outer coating from the fiber using stripper.
- Cleave the fiber end at right angles with 90º using clipper and clean the fiber ends with tissue and alcohol.
- Align the fiber ends in V- groove in fusion splicing machine precisely with a small gap in between the fibers.
- Press the set, the splicing motors will align the fiber ends and Arc fusion will start.
- Check the quality of splicing by measuring the output power for the obtained spliced fiber.
- Protect the splice region through the use of a heat shrink protector or a mechanical crimp protector.

Fusion splicer Fujikura (FSM-60S) has been used in the experiments for splicing CF with (SMF-28), figure (2.10) shows the

photograph of (FSM-60S) fusion splicer (by Fujikura Company). Specifications of arc fusion splicer are shown in appendix (G).

Figure 2.10. Optical fiber arc fusion splicer type (FSM-60S)

The above steps was repeated with 4 cm and 2 cm to prepare three SCS structures with three different CF length.

2.3.3 Preparation of sucrose solution:

To prepare sucrose solution with 10% concentration, a 10g of sucrose has been weighted out and added to 100 ml volumetric flask. Then, deionized water was added to the graduation line and then stirred using magnetic stirrer until dissolved. This step was repeated to prepare 20%, 30%, 40%, 50%, and 60% sucrose solution concentration. The table 2.4 shows the relation between the concentration and RI of sucrose solution [105].

Table 2.4 Relationship between concentration and RI for sucrose solution [105].

Concentration %	0	10	20	30	40	50	60
Refractive Index	1.3330	1.3478	1.3638	1.3811	1.3997	1.4200	1.4418

2.3.4 Fiber Optics sensor based on multimode interference using CF-MZI setup:

After designed and fabricated the SCS structure, the sensor was tested by studied the influence of two parameters, the length and the diameter. The follows section illustrate the procedures to study the effect of those parameters on the sensitivity of the CF-MZI sensor. Three different lengths of CF: 2, 4 and 6 cm were used in the experiments to exploit the change in concentration/ RI at the wavelength shift with. Different fluids (air, water, Acetone, and Hexane) at different refractive indices as shown in table 2.5 used to test SCS structure within the variation in refractive indices.

Table 2.5 Refractive index of used materials at room temperature [106].

Material	Refractive Index
Air	1.0000
Water	1.3333
Acetone	1.3514
N-Hexane	1.3720

2.3.4.1 The influence of the CF length on the sensitivity procedure:

A 6 cm length of etched CF was spliced between two sections of SMF. The experimental setup of the proposed all-fiber MZI is depicted in Figure 2.11
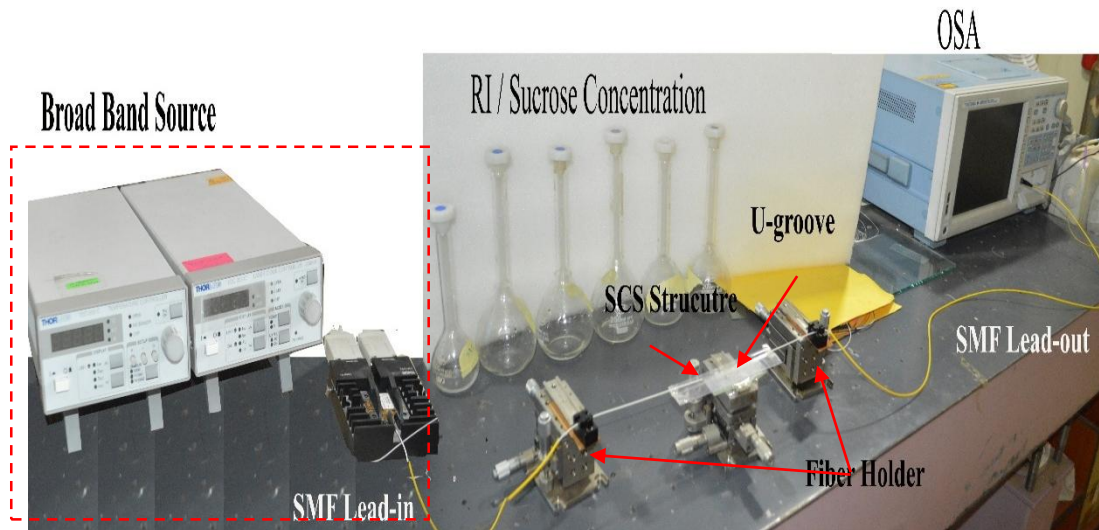
Figure 2.11. Experimental setup of all-fiber CF MZI sensor

The transmission measurement setup for the proposed sensor was carried out using a broadband source (Thorlabs) with wavelength range 1500-1600 nm and YOKOGAWA AQ6370C optical spectrum analyzer (OSA) with resolution of 0.02 nm. The broadband source was connected to CF MZI, while the other end of the CF MZI was connected to the OSA as shown in figure 2.11. The CF MZI structure is fixed using bare fiber holder to avoid the impact of fiber bending or strain on the transmission spectral characteristics of all-fiber sensor. Then the CF MZI has been immersed in deionized water (with refractive index of 1.333) which acts as a cladding for CF instead of air and record the result using OSA. Then, chemical liquids (Acetone, and N-hexane) has been tested. The SCS structure was cleaned and dried post each sensing procedure using

deionized water and dry air. The result wavelength shift and sensitivity was recorded. The above procedures was repeated with 2 cm and 4cm of CF length.

2.3.4.2 The influence of the CF diameter on the sensitivity procedure:

The SCS structure with 4 cm of the CF length was etched to 100 μm. The experimental setup as shown in figure 2.11. The CF MZI structure is fixed using bare fiber holder to avoid the impact of fiber bending or strain on the transmission spectral characteristics of all-fiber sensor. Then the CF MZI has been immersed in deionized water (with refractive index of 1.333) which acts as a cladding for CF instead of air and record the result using OSA. Then, chemical liquids (Acetone, and N-hexane) has been tested. The result wavelength shift and sensitivity was recorded. The above procedures was repeated with 80 μm, and 60 μm, of CF diameter.

2.3.4.3 The influence of the concentration on the sensitivity procedure:

The SCS structure with 4 cm of the CF length was etched to 100 μm. The experimental setup as shown in figure 2.11. The CF MZI structure is fixed using bare fiber holder to avoid the impact of fiber bending or strain on the transmission spectral characteristics of all-fiber sensor. Then the CF MZI has been immersed in deionized water (with refractive index of 1.333) which acts as a cladding for CF instead of air and record the result using OSA. Then, the concentration of the surrounding liquid was increased by adding weighted sucrose to the deionized water (as described in previous subsection). Finally, the concentration of sucrose-water solution was changed from 10% to 60%, with 10% step corresponding to refractive index range from 1.3479 to 1.4418.

For each measurement of specific concentration value, a thin dropper was used to drop a small quantity of the sucrose solution into the

U-shape groove until the sensing element is totally immersed. During consecutive tests, the CF- MZI structure was cleaned with deionized water and dried in air after each concentration measurement. The above steps were repeated with 4 cm and 2 cm.

2.3.4.4 The Flow chart of the experimental procedures

The experimental procedures illustrate as a flow chart in figure 2.12
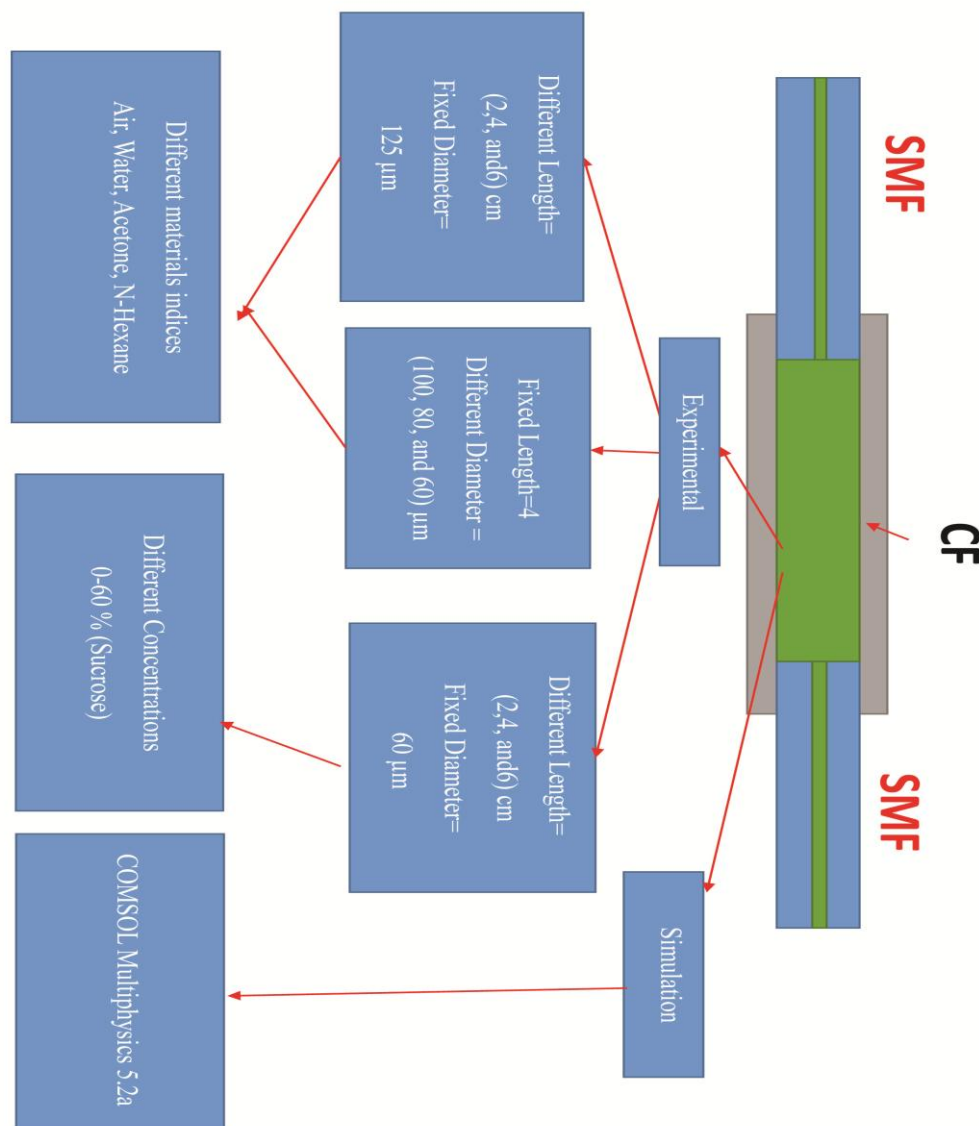
Figure 2.12. Experimental procedures flow chart.

2.3.5 Simulated Modeling:

By using COMSOL Multiphysics program version 5.2a was used to study the effect of CF diameter reducing on the mode field distribution. The 2D Wave optics Module was used with Electromagnetic Waves, frequency domain physics and mode analysis study.

Figure (2.13) illustrates the procedures of design the CF in the COMSOL multphysics program:-
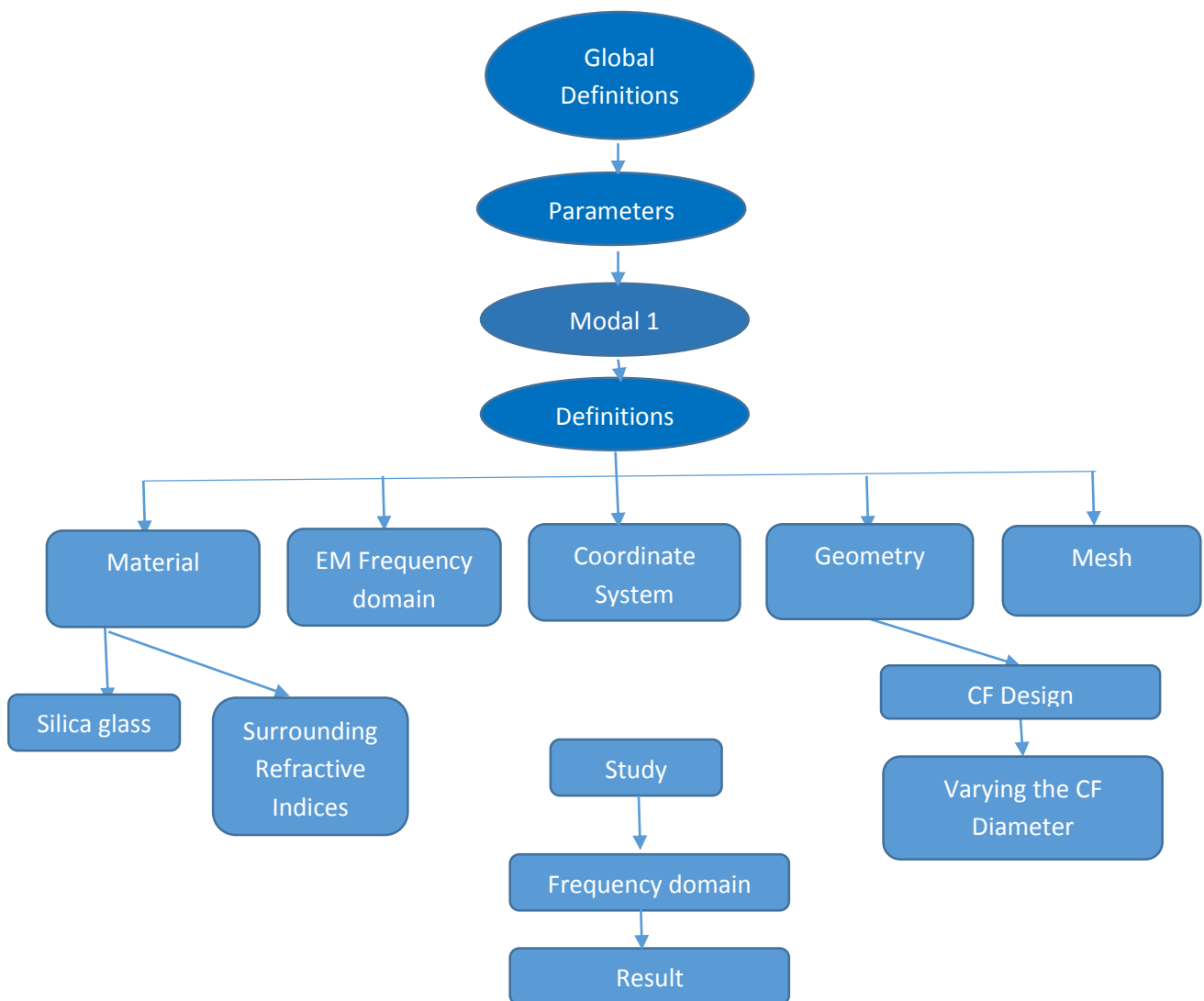
Figure 2.13. illustrates the procedures of design the CF in the COMSOL Multphysics program

Chapter Three

Results and discussion

3.1 Introduction:

Refractive index and concentration CF-MZI sensor has been designed and fabricated. Results, discussion, conclusion, and future work will be presented in this chapter.

The experiments were carried out under the 0.02 nm resolution of the optical spectrum analyzer (Yokogawa AQ6370) and broadband light source (1500-1600 nm). The measurements of the parameters (refractive index and concentration) were demonstrated by monitoring the shift occurs for the transmitted spectrum. The influence of the parameters, the length and the diameter of the CF with varied chemical liquid and concentration were studied.

All the results were taken under scientific laboratory conditions at room temperature and humidity. The using of the safety requirements were committed during experiments.

3.2 SCS Structure stability and transmission:

Transmission stability of the broadband (B.B) source firstly was checked to ensure later accurate measurements (Figure 3.1 bold black curve). Both ends of singlemode fiber was connected to B.B. source and OSA. Figure 3.2 shows the schematic of setup. The second run was carried out with SCS structure at 125 μm CF diameter. The SCS structure acts as bandpass filter where some wavelengths were filtered out because of MMI effect with low loss insertion (~ -9) dBm (Figure 3.1 bold red curve).

Since CF piece was spliced between two segments of SMFs, there were fundamental mode from SMF spilted into multimode and coupled at the

splicing region. The interference occurs between those modes due to multimode interference effect.
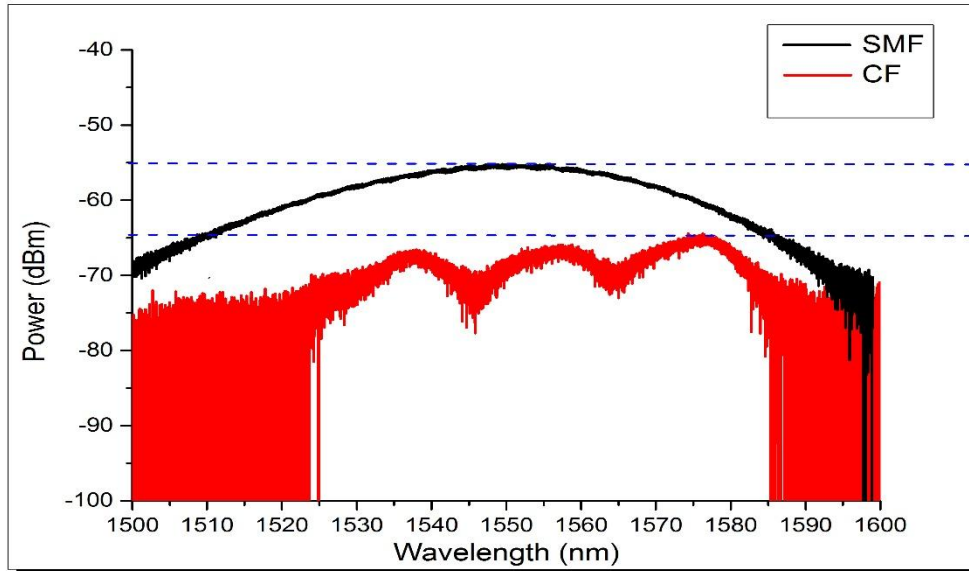
Figure 3.1. B.B. source transmission with Insertion loss of SMF and SCS.
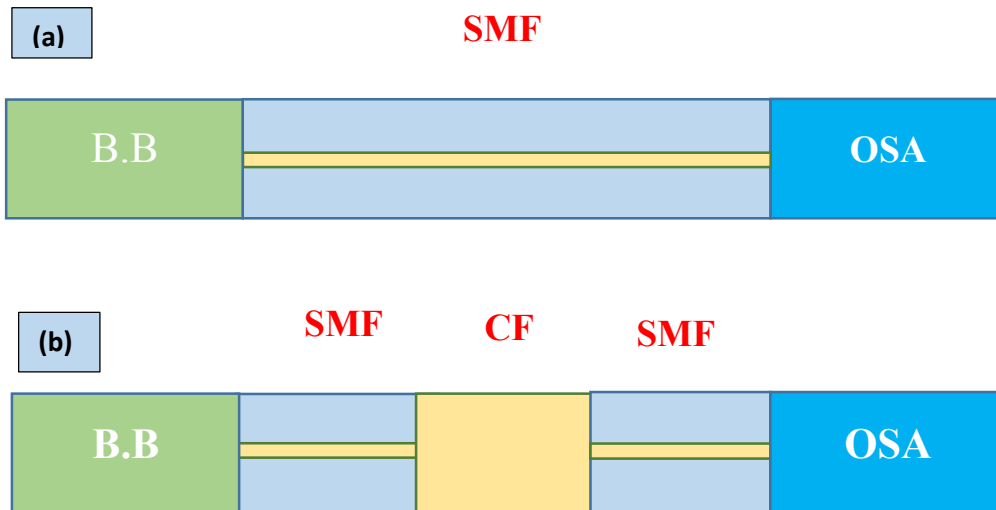
Figure 3.2. Schematic of setup (a) SMF, (b) SCS.

3.3 The Influence of CF length on the sensitivity of CF MZI Sensor

The influence of CF length on CF MZI sensitivity was studied in this work by using different lengths with fixed diameter of CF at 125 μm. The SCS structure was prepared by cleaving CF ends of three lengths (2, 4, and 6) cm. Cleaved CF was spliced to SMF using fusion splicer with automated mode. Different material refractive indices was used to study the change in wavelength shift as a function of refractive index used in this experiment as follows:

3.3.1 2 cm CF length CF MZI Sensor:

2 cm of CF length was used in this experiment with four different refractive indices material (air, water, Acetone, and N-hexane). Figure 3.3 shows variation of the transmitted power with wavelength. The black color is for air, the red for water, the green for Acetone, and purple for N-Hexane. The highest shift was at N-hexane with wavelength shift of 18.34 nm and maximum sensitivity of 150.59 nm/RIU.
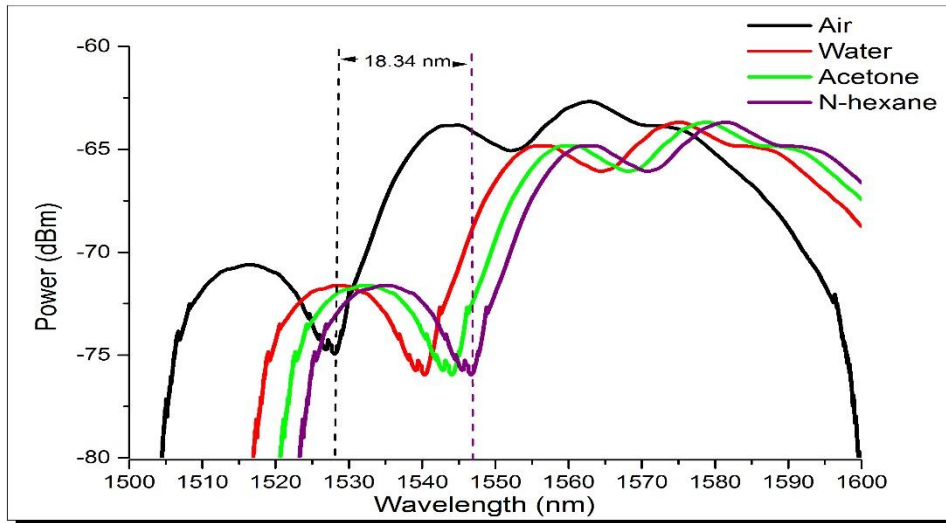
Figure 3.3. Experimental output power versus wavelengths for 2 cm length of CF

3.3.2 4 cm CF length CF MZI Sensor:

4 cm of CF length was used in this experiment with four different refractive indices material (air, water, Acetone, and N-hexane). Figure 3.4 shows variation of the transmitted power with wavelength. The black color is for air, the red for water, the green for Acetone, and purple for N-Hexane. The highest shift was at N-hexane with wavelength shift of 18.34 nm and maximum sensitivity of 150.59 nm/RIU.
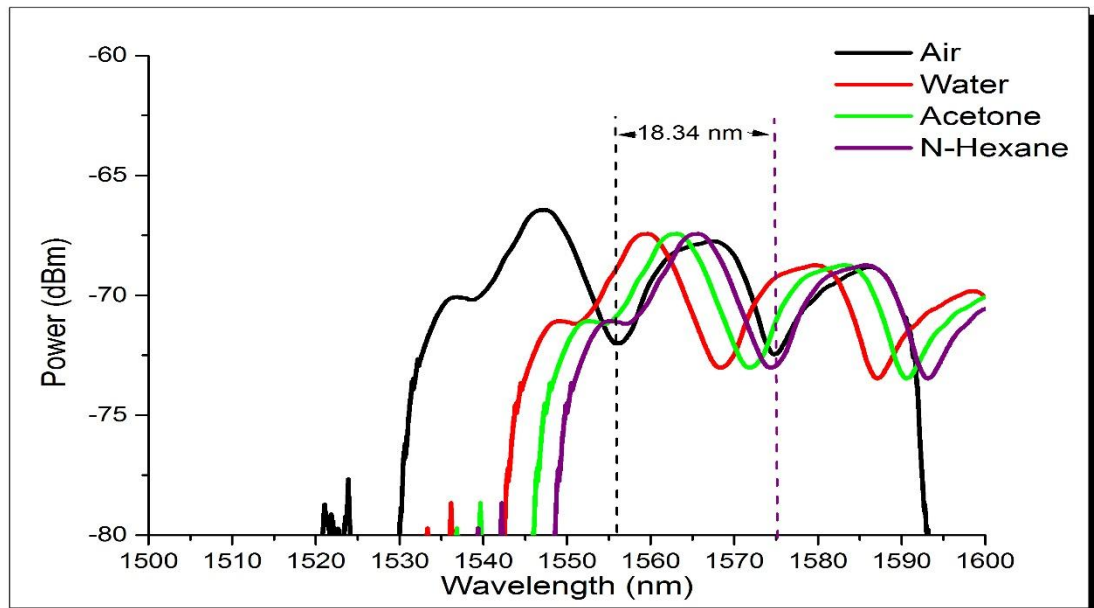
Figure 3.4. Experimental output power versus wavelengths for 4 cm length of CF

3.3.3 6 cm CF length CF MZI Sensor:

6 cm of CF length was used in this experiment with four different refractive indices material (air, water, Acetone, and N-hexane). Figure 3.5 shows variation of the transmitted power with wavelength. The black color is for air, the red for water, the green for Acetone, and purple for N-Hexane. The

highest shift was at N-hexane with wavelength shift of 18.339 nm and maximum sensitivity of 150.57 nm/RIU
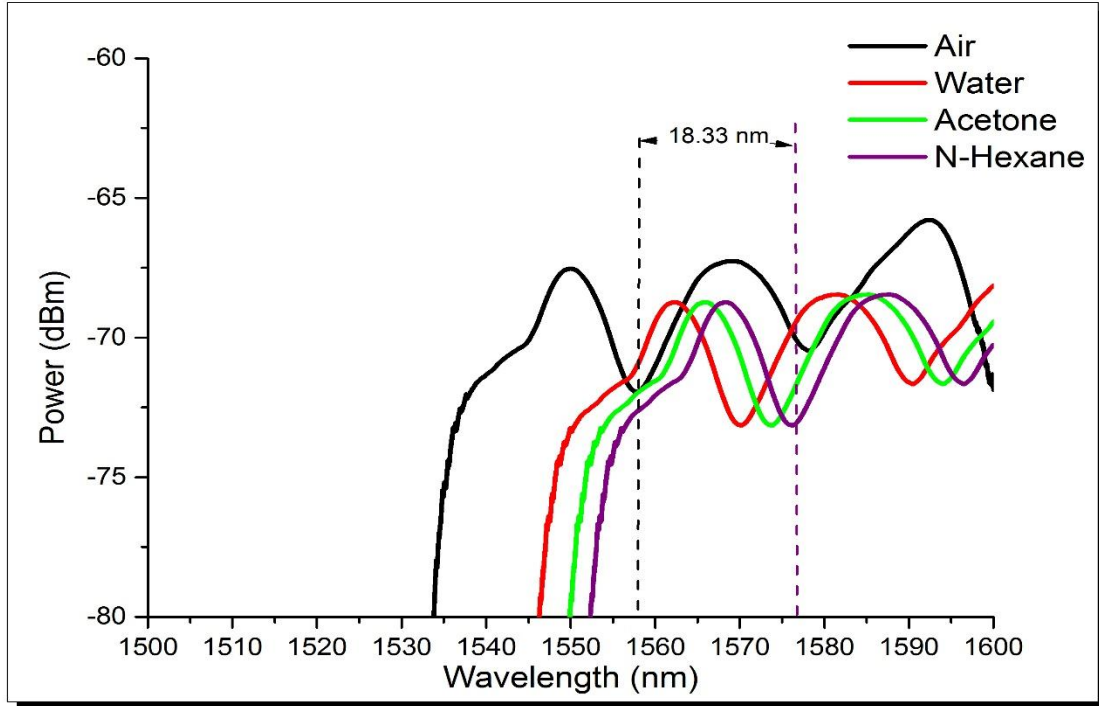
Figure 3.5. Experimental output power versus wavelengths for 6 cm length of CF

3.3.4 Relationship between CF length and Sensitivity

 From figures (3.3,3.4, and 3.5), the wavelength dips were shifted towards red shift when the refractive index increases from 1 in air to 1.3751 in hexane. Figure 3.6 shows the relationship between the variations in CF length with wavelength shift. From figure 3.7, the sensitivity and wavelength has no remarkable change with the variation of the length of the CF when outer diameter of CF was fixed at 125 μm. This might be due to the self-imaging effect in MMI.
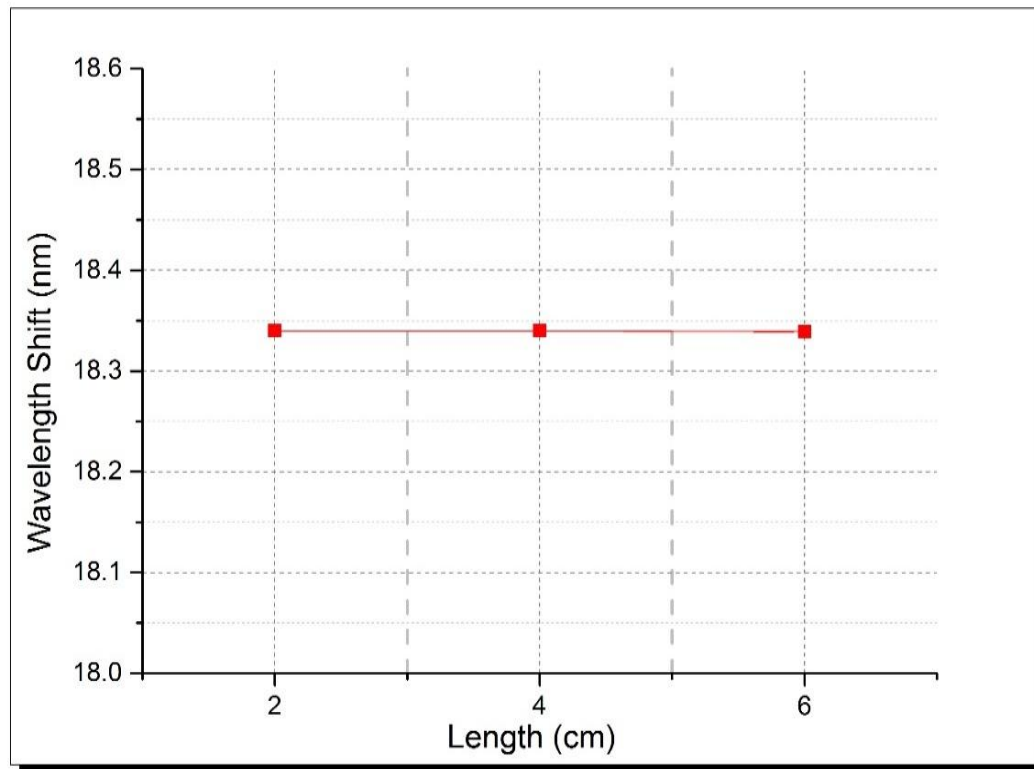
Figure 3.6. Wavelength Shift (nm) as a function of CF Length
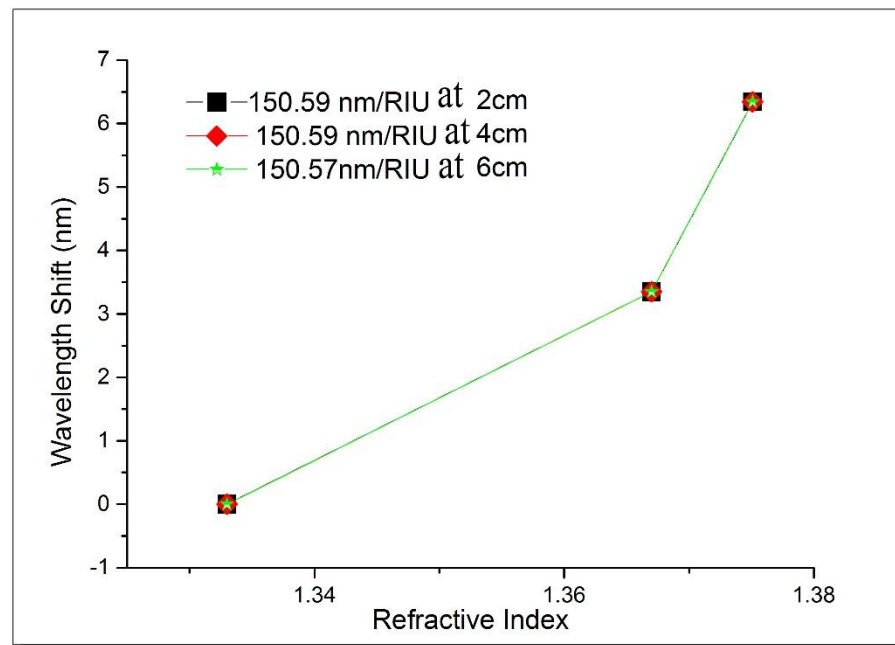
Figure 3.7. Wavelength Shift (nm) as a function of RI at different CF lengths at fixed CF diameter 125 µm

3.4 The Influence of CF Diameter on the sensitivity of CF MZI Sensor

The influence of CF Diameter on CF MZI sensitivity was studied in this experiment by using different diameters of CF with fixed length. Since there is no noticeable change on the sensitivity when the length is changed, then the length is fixed at 4 cm because of the easy of fabrication and handling.

The SCS structure was prepared by cleaving 4 cm length CF ends. Cleaved CF was spliced to SMF using fusion splicer with automated mode. The SCS structure is has been etched using HF (40%) to decrease the outer diameter of CF from 125 μm to 100, 80, and 60 μm respectively.

Different fluids with different refractive indices were investigated. The wavelength shift as a function of refractive index was demonstrated experimentally.

3.4.2 100 μm CF diameter CF MZI Sensor:

After reducing the CF diameter to 100 μm by etching, a fixed CF length of 4cm was used in the SCS structure. Four different material with different refractive indices have been tasted as shown in figure 3.8. The spectrum with black color red, green, and purple represent air medium, water, Acetone and N-Hexane respectively. The maximum shift was at N-hexane with wavelength shift of 23.09 nm and maximum sensitivity of 208.78 nm/RIU.
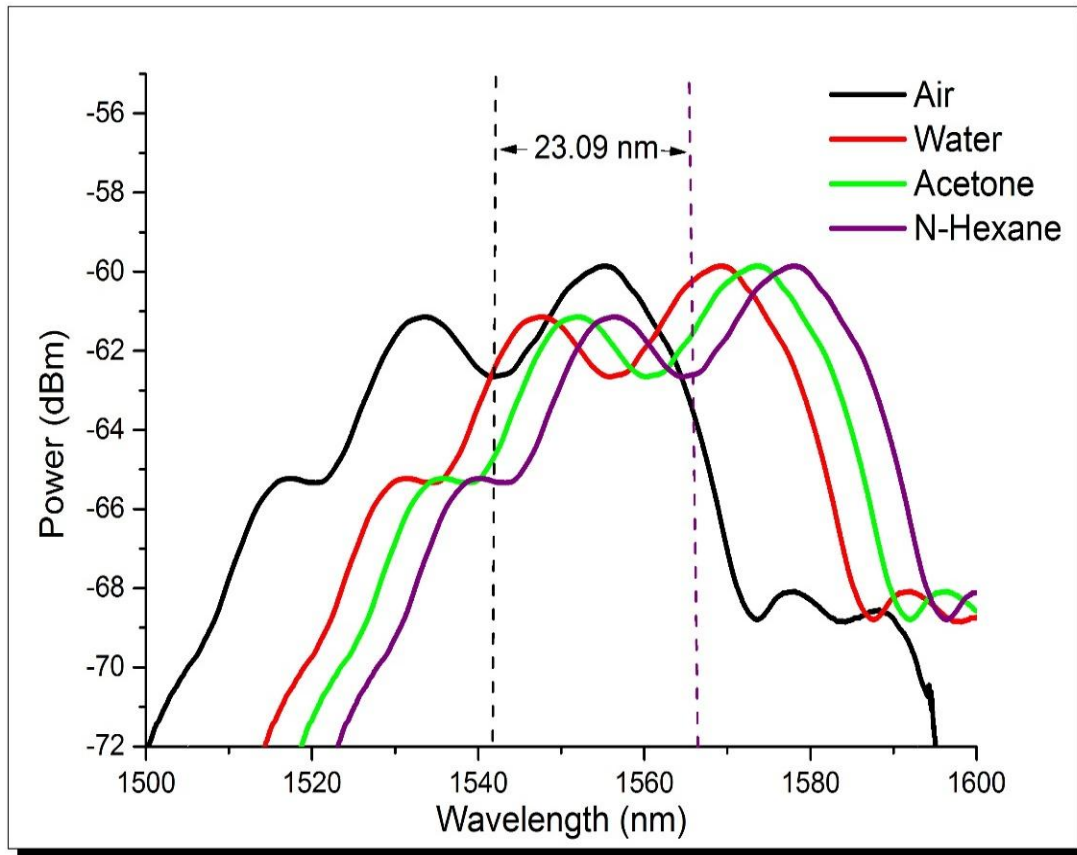
Figure 3.8. Experimental output power versus wavelengths for 100 µm diameter of CF

3.4.3 80 µm CF diameter CF MZI Sensor:

After reducing the CF diameter to 80 µm by etching, a fixed CF length of 4cm was used in the SCS structure. Four different material with different refractive indices have been tasted as shown in figure 3.9. The spectrum with black color red, green, and purple represent air medium, water, Acetone and N-Hexane respectively. The maximum shift was at N-hexane with wavelength shift 24.29 nm and maximum sensitivity 212.58 nm/RIU.
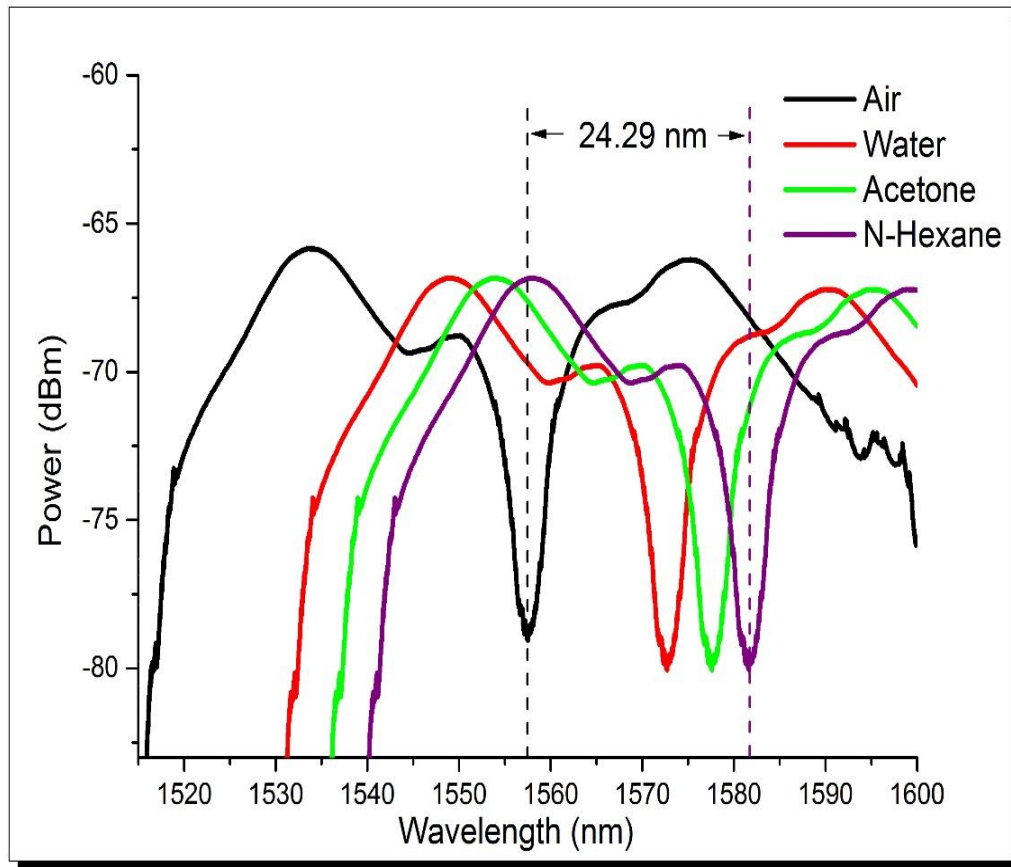
Figure 3.9. Experimental output power versus wavelengths for 80 µm diameter of CF

3.4.4 60 µm CF diameter CF MZI Sensor:

After reducing the CF diameter to 60 µm by etching, a fixed CF length of 4cm was used in the SCS structure. Four different material with different refractive indices have been tasted as shown in figure 3.10. The spectrum with black color red, green, and purple represent air medium, water, Acetone and N-Hexane respectively. The maximum shift was at N-hexane with wavelength shift 30.65 nm and maximum sensitivity   340.85 nm/RIU.
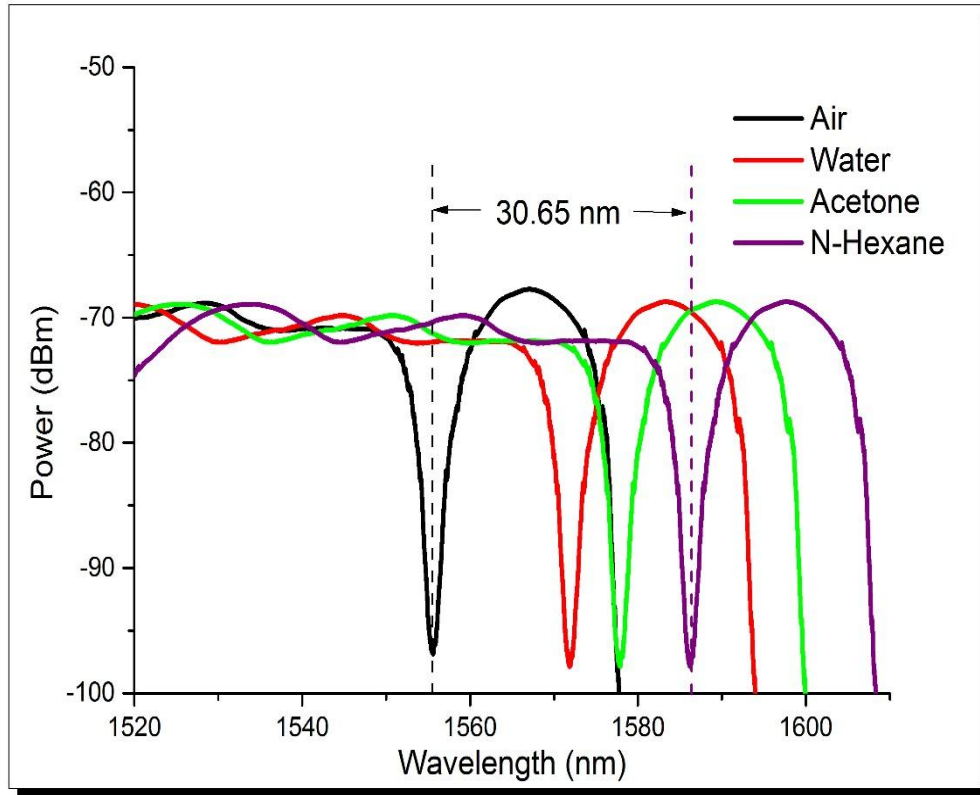
Figure 3.10. Experimental output power versus wavelengths for 60 μm diameter of CF

3.4.5 Effect of the CF diameter on the Sensitivity

From figures (3.3, 3.8, 3.9, and 3.10), the wavelength dips have red shift when refractive index increases from 1 in air to 1.3751 in hexane. Figure 3.11 shows the relationship between the varied in CF diameter with wavelength shift. The sensitivity increases from 150.831 nm/RIU to 340.89 nm/RIU when diameter of CF decreased from 125 μm to 60 μm with fixed CF length at 4 cm as shown in figure 3.12. Since decreasing the diameter allows more interaction of evanescent wave with surrounding refractive index those to self-imaging effect in MMI [87]. The change in refractive index due to the change the effective refractive index (n_{eff}) of the interfering cladding mode propagating in the CF the modulation of the (n_{eff}) occurs which accordingly lead to change the position

of the interference pattern. Also the maximum shift increases depending on the diameter etching [96].
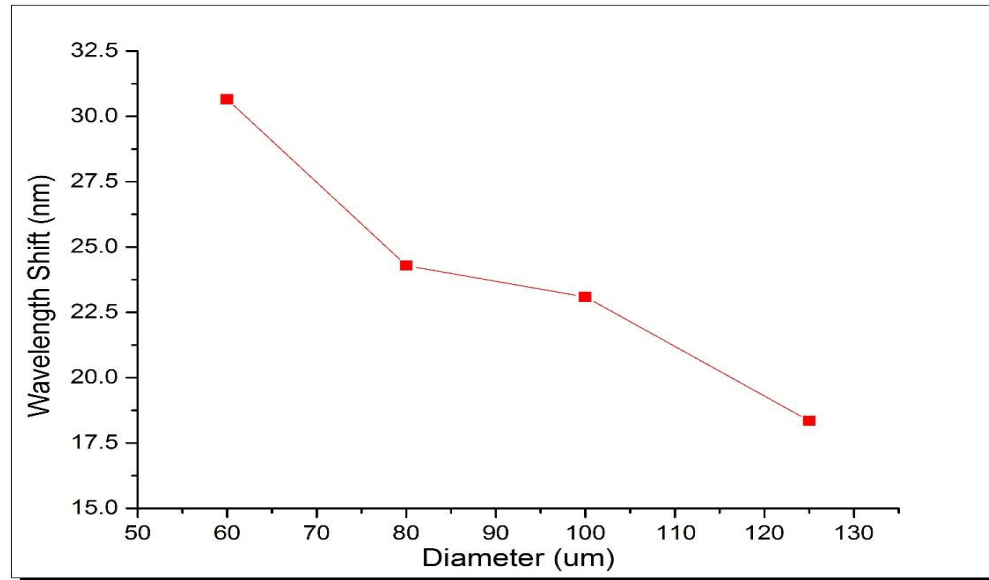
Figure 3.11. Wavelength Shift (nm) as a function of CF Diameter at 4 cm of CF length
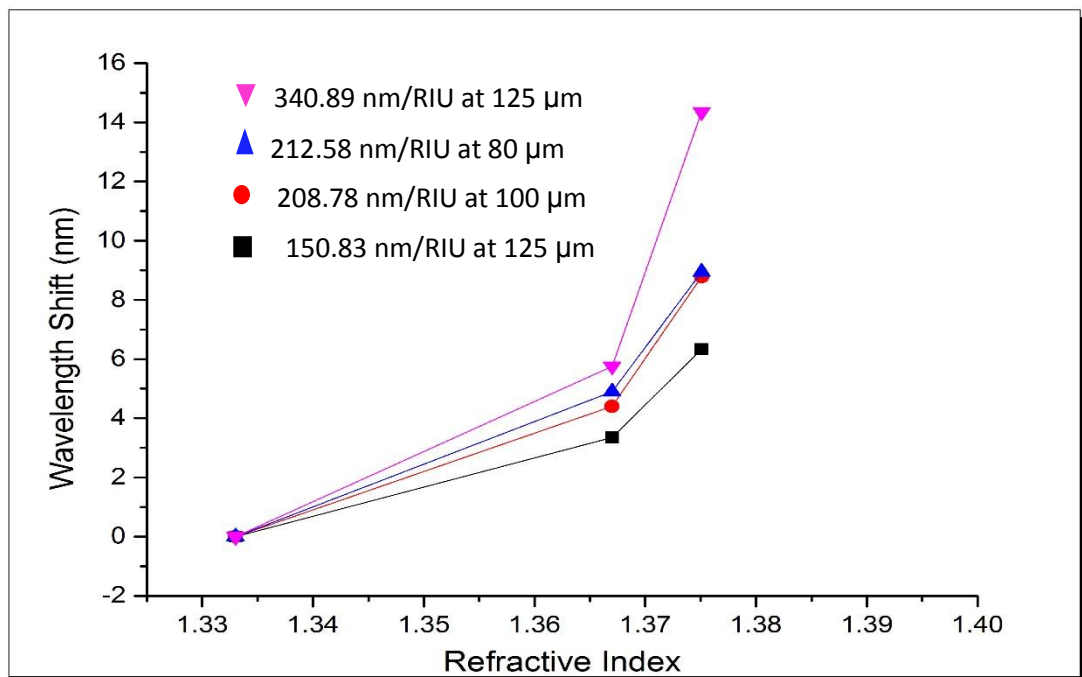
Figure 3.12. Wavelength Shift (nm) as a function of RI at different CF Diameters

3.5 The SCS CF- MZI Concentration Sensor:

Sucrose is a natural product extracted from sugar beet or sugarcane which playing an important role in human health and his nutrition as well it is widely used as a raw material in different food industries [29]. Documentation of sucrose concentration index is very important on paper-marking, food industry, chemical, and sugar production process [30]. Therefore, developing more efficient liquid concentration measurement techniques to improve the production control and the qualities of products is very essential. From aforementioned experiments, when outer diameter of CF decreased, the sensitivity increased. The maximum shift and maximum obtained sensitivity were recorded when CF outer diameter was at 60 μm. The CF MZI sensor in this experiment was used to measure the wavelength shift as a function of sucrose concentration with varied concentration from 0 to 60%. Different lengths of CF at fixed diameter with 60 μm were used to perform the experiments:

3.5.1 The 2 cm SCS CF- MZI Concentration Sensor:

Different sucrose concentration have been prepared and tasted using 2 cm of CF length and 60 μm diameter within the SCS structure. Figure 3.13 the spectrum with black color is indicted to air medium while other colors are for different concentrations of sucrose from 0 to 60% by 10% step. The maximum shift obtained at 60% concentration at 47.7 nm with the sensitivity of 0.52 nm/% (285.79 nm/RIU corresponding to RI).
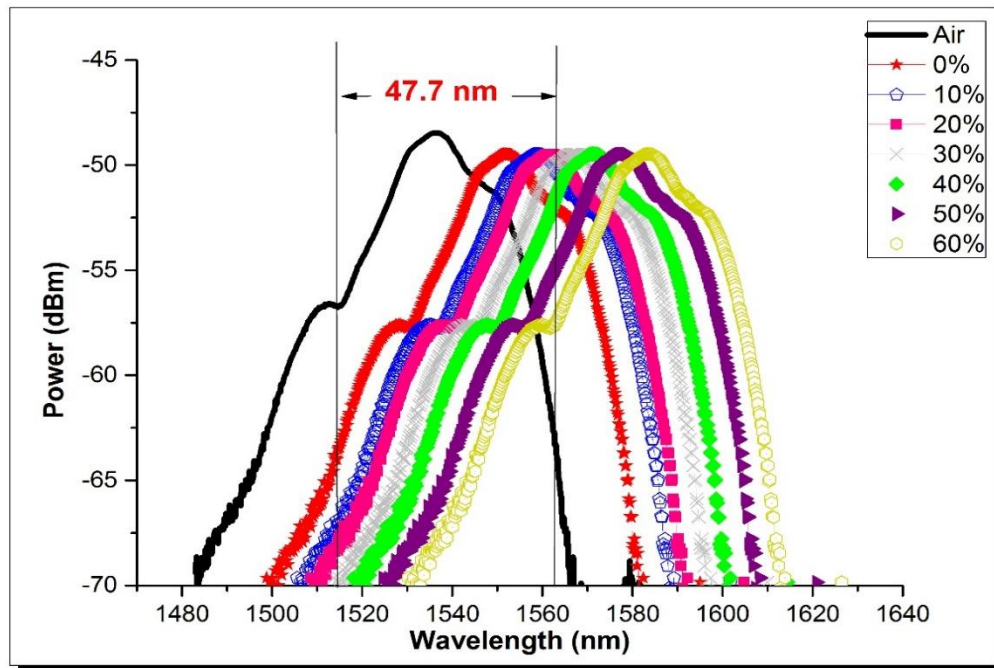
Figure 3.13. Experimental output power versus wavelengths for CF length = 2 cm and diameter = 60 µm

3.5.2 The 4 cm SCS CF- MZI Concentration Sensor:

Different sucrose concentration have been prepared and tasted using 4 cm of CF length and 60 µm diameter within the SCS structure. Figure 3.14 the spectrum with black color is indicted to air medium while other colors are for different concentrations of sucrose from 0 to 60% by 10% step. The maximum shift obtained at 60% concentration at 44.1 nm with the sensitivity was 0.485 nm/% (265.92 nm/RIU corresponding to RI).
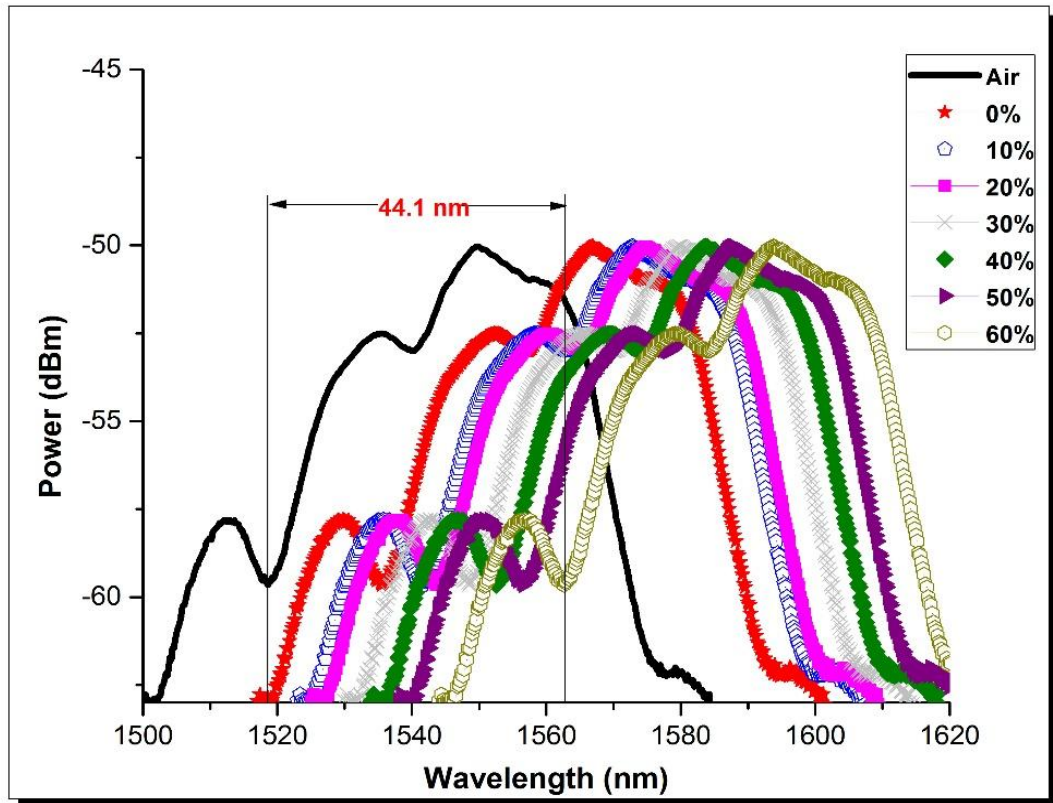
**Figure 3.14. Experimental output power versus wavelengths for CF length
= 4 cm and diameter = 60 μm**

3.5.3 The 6 cm SCS CF- MZI Concentration Sensor:

Different sucrose concentration have been prepared and tasted using 6
cm of CF length and 60 μm diameter within the SCS structure. Figure 3.15 the
spectrum with black color is indicted to air medium while other colors are for
different concentrations of sucrose from 0 to 60% by 10% step. The maximum
shift obtained at 60% concentration at 41.7 nm with the sensitivity was 0.46
nm/% (252.8 nm/ RIU corresponding to RI).
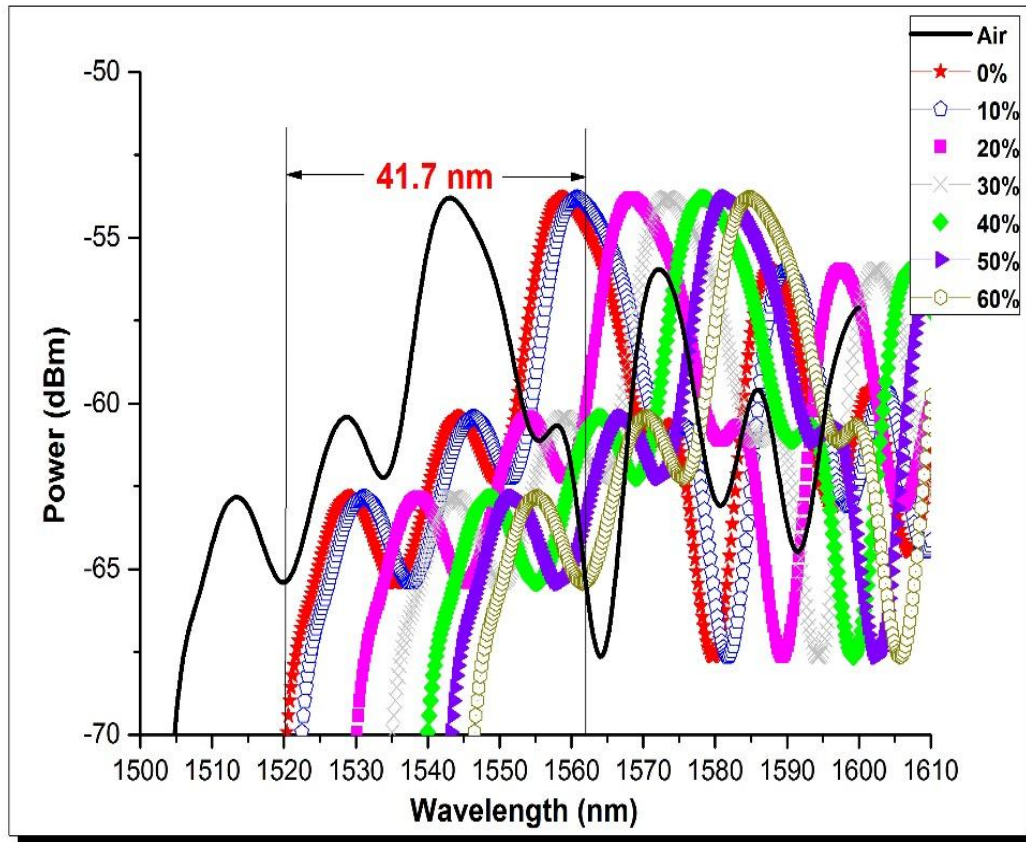
Figure 3.15. Experimental output power versus wavelengths for CF length = 6 cm and diameter = 60 um

3.5.4 Effect of the concentration on the Sensitivity:

Three different lengths of CF composing the Mach-Zehnder Interferometer (2, 4 and 6) cm were used to conduct the experiments to exploit the change in concentration/ RI with the wavelength shifts as shown in Figure 3.13 - Figure 3.15, respectively. It is clear that the red shift is dominated when RI increases. In addition, different lengths of CF gives different output spectral profiles. The relationships between the wavelength shift and the concentration of the surrounding liquid under different lengths of CF are shown in Figure 3.16. The maximum wavelength shifts were 47.1, 44.1 and 41.7 nm for 2, 4 and

6 cm lengths of CF, respectively. This indicates that when the other parameters of the interferometer kept constant, the only key parameter affect the sensitivity is the length of the CF [87].
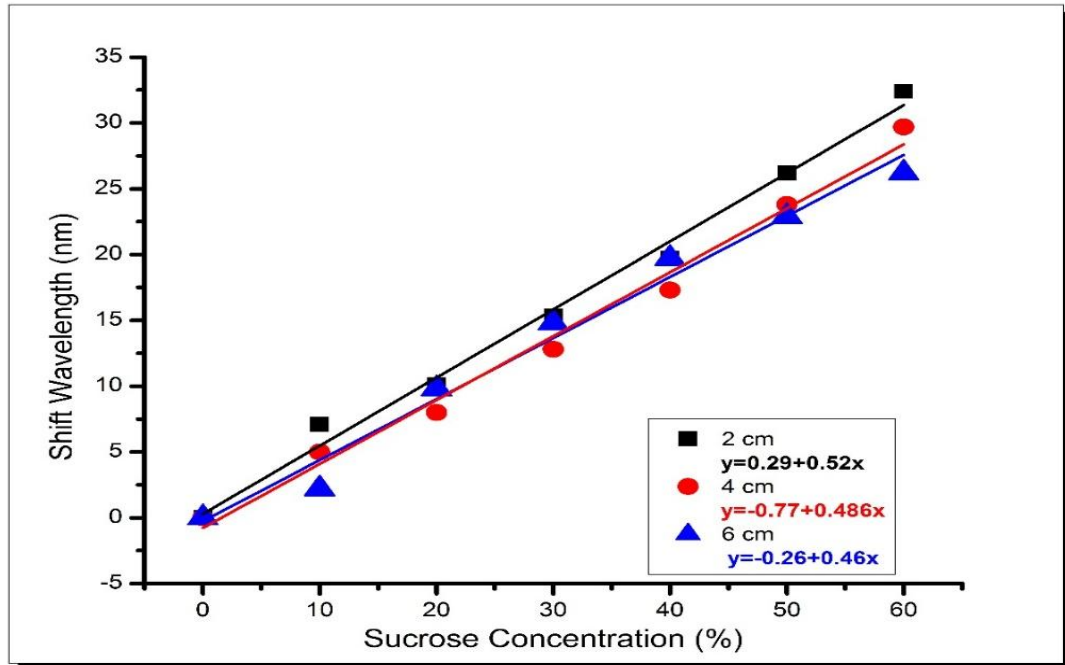
Figure 3.16. Wavelength shift as a function of concentration for different lengths of CF.

The experimental results show the sensitivity will be increased with decreasing the length of Coreless fiber and the decrease of diameter. Fiber diameter decreasing will stimulate more higher order modes which will infiltrate external environment solution, The power of higher order modes are easy to be leaked out into surrounding RI as a form of evanescent wave through the etching region and the contact area between cladding mode evanescent field and external solution increases, so surrounding refractive index changing will influence cladding mode transmission greater, that is to say, it will result in wavelength shift increasing and sensitivity improvement.

3.6 Theoretical results for COMSOL Multiphysics program:

In this section, COMSOL Multiphysics program version 5.2a was used to study the effect of CF diameter reducing on the mode field distribution.

The first step to design by choice the geometry unit at µm, and build up the geometry by select circle with diameter at 125 µm for CF cross section and circle with 300 µm length for environmental variation. The second step was done by adding materials with refractive indices for both above geometry.

Third step was done by applying finer mesh to the geometry (Figure 3.17)

By set the wavelength range (1.5 − 1.6) µm, there were wide range of wavelengths pass throw the geometry. The confinement of the applied modes of CF was varied were the diameter of CF was varied and the arrow plot shows the electric field polarization as shown in figure 3.18. Which shows that, the mode confinement is reduce when the diameter decreased and more mode excited. The result of simulation indicate that when diameter of the CF decrease, more evanescent mode will interacted with environmental RI.
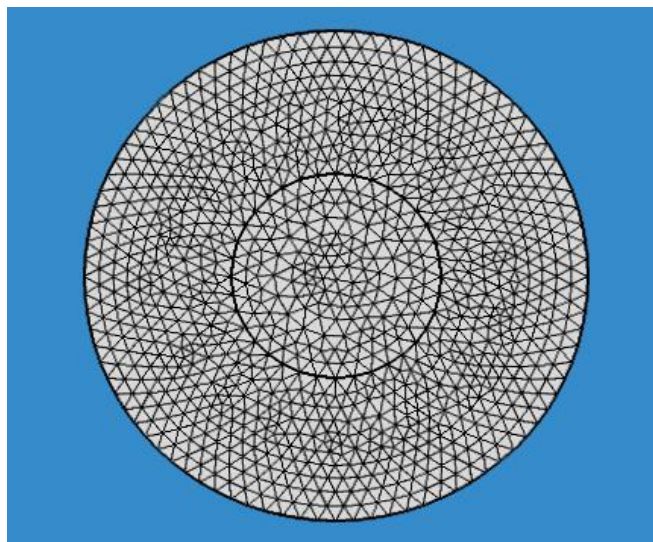
Figure 3.17. CF cross section mesh using COMSOL-mesh finer
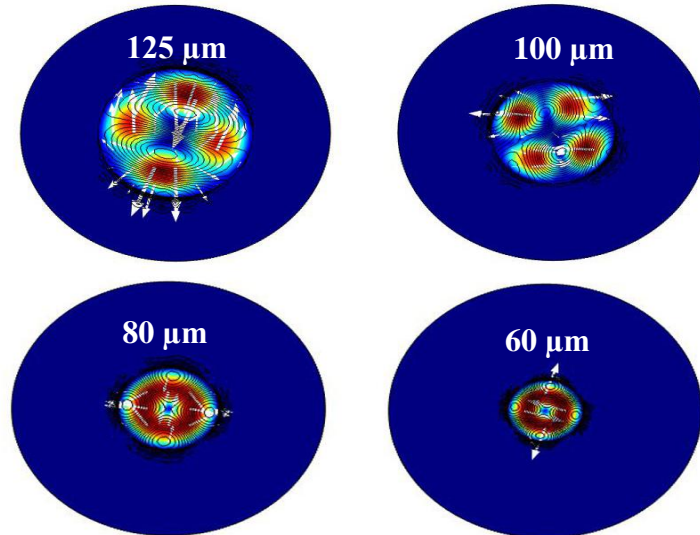
Figure 3.18.Effect of reducing the CF diameter on mode confinement using COMSOL.

The fundamental mode and high order mode appeared when mode-mismatch appeared between SMF and CF since the diameter was different and figure 3.19 shows the modes variation as the diameter of CF varied.
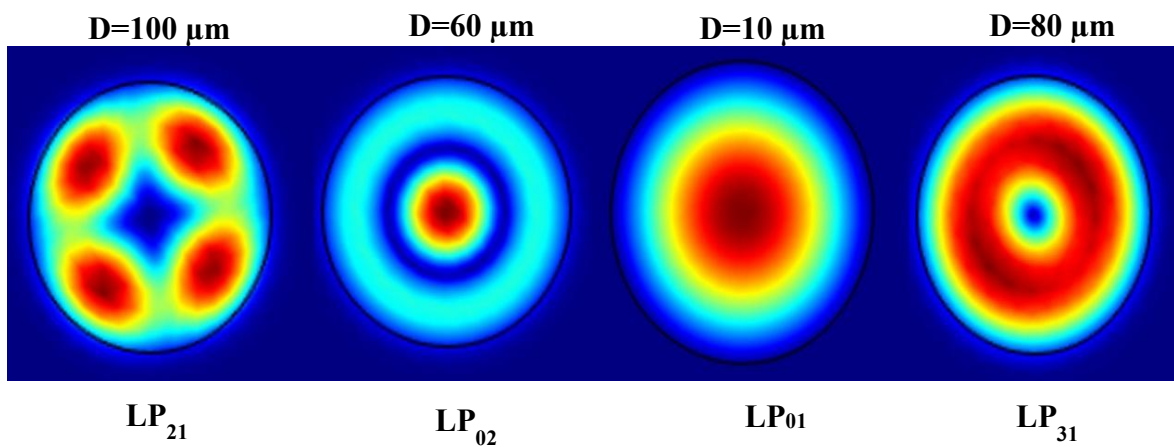
Figure 3.19. Distribution of the Fundamental and High order modes using COMSOL.

3.7 Conclusions

- A highly sensitive concentration / RI sensor based on etching (SCS) fiber structure has been demonstrated experimentally.

- The influence of CF length and diameter was the key control parameter to optimize the sensor performance.

- Length of the CF has no noticeable effect on the concentration / RI sensitivity when the CF diameter at 125 µm.

- The obtained sensitivity has been improved when the diameter of the CF etched from 125 µm to 60µm and obtained wavelength shift will increase toward red shift.

- A maximum wavelength shift at 30.89 nm and maximum obtained sensitivity at 340.85 nm/RIU when diameter of the CF decreased to 60 µm with 4 cm at using different fluids.

- The obtained wavelength shift will increase toward red shift when the sucrose concentrations increase 0-60 %.

- The maximum obtained wavelength shift was 47.1 nm when the diameter of the CF fixed at 60 µm and the length of the CF at 2 cm with maximum obtained sensitivity at 0.52 nm/% (285.79 nm/RIU corresponding to RI) at 60% of sucrose concentration.

- The obtained results showed that the designed concentration / RI sensor sensitivity could be optimized by shortening the length of the CF and reducing the CF outer diameter within the experiment's conditions.

- This sensor has many advantage such as high sensitivity in real time, ease to fabricate, low cost, small and compact.

- This fiber SCS structure seems suitable as fiber based sensor for refractive index at different concentrations with different CF diameters and lengths.

.

3.8 Future work

This work can be extended in the future to cover the following research trends:

1- Using etching CF-MZI at 60 µm with fiber laser system as tunable filter.

2- Spliced PCF fiber with etching CF-MZI to fabricate a dual measurements sensor for Temperature and refractive index parameters.

3- Using another liquids with different concentrations instead of sucrose concentration liquid.

4- Using etching CF-MZI in chemical liquids systems for liquid level sensing and also gas sensing.

3.9 References

[1] A. Norouzi, A. H. Zaim, and B. B. Ustundag, "An integrated survey in Optical Networks: Concepts, Components and Problems", 11, 1, pp. 10-26, (2011).

[2] S. C. Huang, W. W. Lin, M. T. Tsai, and M. H. Chen. "Fiber optic in-line distributed sensor detection and localization of the pipeline leaks". Sensors and Actuators A, 135, pp. 570–579, (2007).

[3] P. A. E. Piunno, U. J. Krull, R. H. E. Hudson, M. J. Damha, and H. Cohen. "Fiber optic biosensor for fluorimetric detection of DNA hybridization". Analytica Chimica Acta, 288, 3, pp. 205–214, (1994).

[4] J. Wang, and J. Tang "Photonic crystal fiber Mach-Zehnder interferometer for refractive index sensing". Sensor 12: 2983-2995 (2012).

[5] S. Qiu, Y. Chen, F. Xu, and Y. Lu " Temperature sensor based on an isopropanol-sealed photonic crystal fiber in-line interferometer with enhanced refractive index sensitivity" Optics Letters, 37, 5, pp. 863-865, (2012).

[6] T. Kumagai, H. Soekawa, T. Yuhara, and H. Kajioka. "Fiber optic gyroscopes for vehicle navigation systems". Proceedings of SPIE, 2070:181–191, (1994).

[7] M. Batumalay, S.W.Harun, N. Irawati, H.Ahmad and H. Arof "A Study of Relative Humidity Fiber-Optic Sensor". IEEE Sensors Journal, 15, 3, pp. 1945-1950, (2015).

[8] L. Ma, Y. Qi, Z. Kang, and S. Jian, "All-Fiber Strain and Curvature Sensor Based on No-Core Fiber". IEEE Sensors Journal, 14, 5, pp. 1514-1517, (2014).

[9] J. Ballato, "The Carrier of Light – A Brief History of Optical Fiber", Journal of Applied Glass Science, 7, 4, pp. 413-422, (2016).

[10] R. Buczynski, "Photonic Crystal Fibers", Acta Physica Polonica A, 106, 2, pp. 141-167, (2004).

[11] J. A. Bebbington, G. Barbarossa, J. R. Bonar, and J. S. Aitchison, " Rare earth doped silica waveguides on Si fabricated by flame hydrolysis deposition and aerosol doping " Applied Optics Letter, 62, 4, pp. 337-339 (1993).

[12] S. Choi, T. J. Eom, J. W. Yu, B. H. Lee, and K. Oh, "Novel All-Fiber Bandpass Filter Based on Hollow Optical Fiber", IEEE Photonics Technology Letters, 14, 12, pp. 1701-1703, (2002).

[13] F. S. Delgado, J. P. Carvalho, T. V. N. Coelho and Al. B. Dos Santos, "An Optical Fiber Sensor and Its Application in UAVs for Current Measurements", Sensor, 16,11, ID 1800, pp.1-8 (2016).

[14] A. Aslian, B. Honarvar S. Asli, C. J. Tan, F. R. Adikan, and A. Toloei, "Design and Analysis of an Optical Coupler for Concentrated Solar Light Using Optical Fibers in Residential Buildings", Journal of Photoenergy, 2016,ID 3176052, pp.1-11, (2016).

[15] J.S. Krasiñski and G.W. Pearson, "Optical Nonreciprocal Devices and Their Applications", Proceedings of the International Conference "Quantum Optics III", Szczyrk, Poland, 1993.

[16] C. Han, H. Ding, and F. Lv, "Demonstration of a refractometric sensor based on an optical micro-fiber three-beam interferometer", Scientific Reports 4, 7504, pp. 1-7, (2014).

[17] X. Wang, X. Wu, S. Li, Q. Ge, T. He, and B. Yu, "Fiber-optic accelerometer based on a modal interferometer using a thin-core fiber", Optica Applicata, XLV, 3, pp. 317-325, (2015).

[18] R. Kashyap,and B. K. Nayar, "An all single-mode fiber Michelson interferometer sensor", Journal of Lightwave Technology, 1,4, pp. 691-624, (1983).

[20] X. Jin, X. Huang, and L. Chen, "An Extrinsic Fabry–Perot Optical Fiber Sensor Based on Nano-Magnetic Fluid", Fiber and Integrated Optics 32, pp. 233–24, (2013).

[21] D. Yuan, Y. Dong, Y. Liu, and T. Li, "Mach-Zehnder Interferometer Biochemical Sensor Based on Silicon-on-Insulator Rib Waveguide with Large Cross Section", Sensors, 15, 9, pp. 21500-21517, (2015).

[22] Y. Li, Z .Liu, and S. Jian, "Multimode Interference Refractive Index Sensor Based on Coreless Fiber", Photonic Sensors, 4, 1, pp. 21-27, (2014).

[23] H. Y. Choi, M. J. Kim, and B. H. Lee, "All-fiber Mach-Zehnder type interferometers formed in photonic crystal fiber", Optics Express, 15, 9, pp. 5711-5720, (2007).

[24] R. M. Chyad, M. Z. M. Jafri, and K. Ibrahim, "Fabricated nano-fiber diameter as liquid concentration sensors", Results in Physics, 3, pp. 91–96 (2013).

[25] R. Zhao, T. Lang, J. Chen, and J. Hu, "Polarization-maintaining fiber sensor for simultaneous measurement of the temperature and refractive index". Optical Engineering, 56, 5, ID 057113, pp. 1-5, (2017).

[26] Z. Wu, X. Yu, E. Gu, Z. Kong, and W. Li, " Characteristics analysis of chemical concentration sensor based on three-layer FBG. Optics and Photonics Journal, 3, pp. 268-271, (2013).

[27] Y. Zhao, L. Cai, X. Li, and F. Meng, "Liquid concentration measurement based on SMS fiber sensor with temperature compensation using an FBG. Sensors and Actuators B, 196, pp. 518-524, (2014).

 [28] J. Zhang, W. Chen, and C. Dong,"Fiber-optic sucrose sensor based on mode-filtered light detection", Journal of Carbohydrate Chemistry, 32, pp. 475-482, (2013).

[29] W.A. Khaleel, and A. H. Al-Janabi, "High-sensitivity sucrose erbium-doped fiber ring laser sensor". Optical Engineering, 56, 2, pp. 0261161-0261166, (2017).

[30] Y. Zhu, H. Wang, and Y. Hsu, "The measurement of sucrose concentration by two-tapered all fiber Mach–Zehnder interferometer employing different coupling structures and manufacture processes". Springer, 23, pp. 662–677, (2016).

[31] J. M. Senior, "Optical Fiber Communications principles and practice", 3rd edition, Prentice Hall, ch2, pp. 26-28, (2009).

[32] G.P. Agrawal, Fiber-Optic Communication Systems, 3rd edition , Jhon Wiley & Sons Inc., ch2 23-36 (2002).

[33] https://www.thorlabs.com/newgrouppage9.cfm?objectgroup_id=1596 2017/09/06.

[34] J. Wang, C. Jiang, W. Hu, and M. Gao, "Modified design of photonic crystal fibers with flattened dispersion", Optics & Laser Technology, 38, 3, pp. 169–172, (2006).

[35] B. Zsigri, "Photonic crystal fibers as the transmission medium for future optical communication systems", Ph. D. Thesis, Research Center COM, Technical University of Denmark, Kgs. Lyngby, Denmark, (2006)

[36] A. M. R. Pinto and M. Lopez-Amo,"Photonic crystal fibers for sensing Applications, "Journal of Sensors, review, 2012, ID 598178, pp.1-12, (2012).

[37] A. Bjarklev, J. Broeng, S.E. Barkou, E. Knudsen, and H.R. Simonsen, "Photonic crystal fiber modelling and applications", Proceedings of Optical Fiber Communication Conference and Exhibit, (2001).

[38] https://www.thorlabs.com/newgrouppage9.cfm?objectgroup_id=7948 2017/09/06.

[39] Y. Liu, Y. Li, X. Yan, and W. Li, "High Refractive Index Liquid Level Measurement via Coreless Multimode Fiber", IEEE Photonics Technology Letters, 27, 20, pp. 2111- 2114, (2015).

[40] J. Villatoro, V. Finazzi, G. Badenes, and V. Pruneri, "Highly sensitive sensors based   on photonic crystal fiber modal interferometers" Journal of Sensors, review, 2009, ID 747803, pp.1-11, (2009).

[41] S. Qiu, Y. Chen, J. Kou, F. Xu, and Y. Lu, "Miniature tapered photonic crystal fiber interferometer with enhanced sensitivity by acid microdroplets etching". Applied Optics 50, 22, ID 144882, pp. 4328-4332, (2011).

[42] C. Zhao, X. Yang, C. Lu, W. Jin, and M. S. Demokan, "Temperature-insensitive interferometer using a highly birefringent photonic crystal fiber loop mirror", IEEE Photonics Technology Letters, 16, 11, pp. 2535–2537, (2004).

[43] L. Alwis, T. Sun, And K.T.V. Grattan, "Optical Fibre-Based Sensor technology for humidity and moisture measurement: Review of recent progress", Measurement, review, 46, 10, pp. 4052–4074, (2013).

[44] Z. Djinovi,M. Tomic, L. Manojlovic,Ž. Lazic, M. M. Smiljanic,"Non-contact Measurement of Thickness Uniformity of Chemically Etched Si Membranes by Fiber-Optic Low-Coherence Interferometry", Proc. 26th International Conference on Microelectronics (Miel 2008), Niš, Serbia , 11-14 May, (2008).

[45] Y. Li-bo, "Fiber Optic Moiré Interferometer", Chinese Physics Letters, 14, 9, pp. 665-667, (1997).

[46] Y. R. Garcia, J. Corres, and J. Goicoechea,"Vibration Detection Using Optical Fiber Sensors", Journal of Sensors, 2010, ID 936487, pp1-12,(2010).

[47] G. A. Cárdenas-Sevilla, F. C. Fávero, and J, Villatoro, "High-Visibility Photonic Crystal Fiber Interferometer as Multifunctional Sensor", Sensors, 13, pp. 2349-2358, (2013).

[48] B. H. Lee, Y. H. Kim , K. S. Park, J. B. Eom, M. J. Kim , B. S. Rho, and H. Y. Choi, "Interferometric Fiber Optic Sensors", Sensors, review, 12,pp. 2467-2486, (2012).

[49] R. Mehra, H. Shahani, and A. Khan, "Mach-Zehnder Interferometer and it's Applications", International Journal of Computer Applications, JCA Proceedings on National Seminar on Recent Advances in Wireless Networks and Communications, pp.31-36, (2014).

[50] J. Du, Y. Dai, G. K. P. Lei, W. Tong, and C. Shu, "Photonic crystal fiber based Mach-Zehnder interferometer for DPSK signal demodulation", Optics Express, 18, 8, pp. 7917-7922, (2010).

[51] J. Hernandez, R. Laguna, E. Rodriguez, J. Ayala, R. Chavez, D. Vazquez, J Garcia, J. Lucio and J. Gutierrez, "A tunable Multi-wavelength Laser Based on a Mach–Zehnder Interferometer with Photonic Crystal Fiber", Laser Physics, 23, ID 055105, pp. 1-5, (2013).

[52] R. K. Zarzoor,and H. J. Taher "Chemical sensor based on a solid-core photonic crystal fiber interferometer", Iraqi Journal of Physics A, 13, 27, PP. 127-143, (2015).

[53] Y. LI, Z. LIU, and S. JIAN, "Multimode Interference Refractive Index Sensor Based on Coreless Fiber", Photonic Sensors, 4, 1, pp. 21–27, (2014).

[54] A. W. Lohmann, H. Knuppertz and J. Jahns, "Fractional Montgomery effect: a self-imaging phenomenon", Jornal of Optical Society of America A, 22, 8, pp. 1500-1508, (2005).

[55] X. Zhu, A. Schülzgen, H. Li, L. Li, L. Han, J. V. Moloney, and N. Peyghambarian, Detailed investigation of self-imaging in largecore

multimode optical fibers for application in fiber lasers and amplifiers" , Optics Express, 16, 21, pp. 16632-16645, (2008).

[56] E. Udd, "An overview of fiber-optic sensors", Review of Scientific Instruments, 66, 8, 4015-4030, (1995).

[57] R. Levy and S. Ruschin, "Design of a Single-Channel Modal Interferometer Waveguide Sensor", IEEE Sensors Journal, 9, 2, pp. 146-153, (2009).

[58] D. Kinet, P. Mégret, K. W. Goossen, L. Qiu , D. Heider and C. Caucheteur, "Fiber Bragg Grating Sensors toward Structural Health Monitoring in Composite Materials: Challenges and Solutions" Sensors, 14, pp. 7394-7419, (2014).

[59] T. S. Mansour, and F. M. Abdulhussein,"Dual Measurements of Pressure and Temperature with Fiber Bragg Grating Sensor", Al-Khwarizmi Engineering Journal, 11, 2, P.P. 86- 91, (2015).

[60] F. Chiavaioli, C. A. J. Gouveia, P. A. S. Jorge, and F. Baldini,"Towards a Uniform Metrological Assessment of Grating-Based Optical Fiber Sensors: From Refractometers to Biosensors", Biosensors, review, 7, 23, pp. 1-29, (2017).

[61] X. Bao, and L. Chen, "Recent Progress in Distributed Fiber Optic Sensors", Sensors, review, 12, pp. 8601-8639, (2012).

[62] Alan Rogers, "Distributed optical-fibre sensing", Measurement Science and Technology, 10, 8, pp. R75–R99, (1999).

[63] Y. Wang, H. Bartelt, S. Brueckner, J. Kobelke, M. Rothhardt, K. Mörl, W. Ecke, and R. Willsch, "Splicing Ge-doped photonic crystal fibers

using commercial fusion splicer with default discharge parameters", Optics Express, 16, 10, pp.7258-7263 , (2008).

[64] K. Borzycki and K. Schuster, "Arc Fusion Splicing of Photonic Crystal Fibres," in Photonic Crystals – Introduction, Applications and Theory, A. Massaro, ed. (InTech, 2012), pp. 175–200, (2012).

[65] R. Thapa, K. Knabe, K. L. Corwin, and B. R. Washburn, "Arc fusion splicing of hollow-core photonic bandgap fibers for gas-filled fiber cells" Optic. Express, 14, pp. 9576-9583, (2006).

[66] S. N. Ismail, H. J. Taher, and A. H. Al-Janabi,"Fusion Splicing for a Large Mode Area Photonic Crystal Fiber with Conventional Single Mode Fiber", Iraqi Journal of Physics A, 13, pp. 9-17 ,(2014).

[67] Y. Wang, H. Bartelt, S. Brueckner, J. Kobelke, M. Rothhardt, K. Mörl, W. Ecke, and R. Willsch, "Splicing Ge-doped photonic crystal fibers using commercial fusion splicer with default discharge parameters", Optics Express, 16, 10, pp. 7253-7263, (2008).

[68] H. Yu, Q. Huang, and J. Zhao, "Fabrication of an Optical Fiber Micro-Sphere with a Diameter of Several Tens of Micrometers", Materials, 7, pp. 4878-4895, (2014).

[69] S. Ko, J. Lee, J. Koo, B. S. Joo, M. Gu, and J. H. Lee, "Chemical wet etching of an optical fiber using a hydrogen fluoride-free solution for a saturable absorber based on the evanescent field interaction", Journal of Lightwave Technology, 34, 16, pp. 3776 - 3784, (2016).

[70] S. Dutta, M. Imran, P. Kumar, R. Pal, P. Datta, and R. Chatterjee, "Comparison of etch characteristics of KOH, TMAH and EDP for bulk

micromachining of silicon (110)", Microsystem Technologies, 17, pp. 1621–1628, (2011).

[71] K. Solehmainen, T. Aalto, J. Dekker, M. Kapulainen, M. Harjanne, K. Kukli, P. Heimala, K. Kolari, and M. Leskelä ,"Dry-etched silicon-on-insulator waveguides with low propagation and fiber-coupling losses", Journal of Lightwave Technology, 23, 11, pp. 3875-3880, (2005).

[72] B. E. E. Kastenmeier, P. J. Matsuo, and G. S. Oehrlein, "Remote plasma etching of silicon nitride and silicon dioxide using NF3/O2NF3/O2 gas mixtures", Vacuum Science & Technology A, 16,4 2047-2055, (1998).

[73] H. Wang, S. Pu, N. Wang, S. Dong, and J. Huang, "Magnetic field sensing based on singlemode–multimode–singlemode fiber structures using magnetic fluids as cladding" Optics Letters, 38,19, pp. 3765-3765, (2013).

[74] L. Xue, and L. Yang, "Sensitivity enhancement of RI sensor based on SMS fiber structure with high refractive index overlay", Journal of Lightwave Technology, 30, 10, pp.1463-1469, (2012).

[75] J. Shi, S. Xiao, L. Yi and M. Bi, "Sensitivity-Enhanced Refractive Index Sensor Using a Single-Mode Thin-Core Fiber Incorporating an Abrupt Taper" , Sensors 2, 12, pp. 4697-4705, (2012).

[76] Roberto Gravina, Genni Testa and Romeo Bernini, "Perfluorinated Plastic Optical Fiber Tapers for Evanescent Wave Sensing", Sensor, 9, 10423-10233, (2009).

[77] R C Kamikawachi, G R C Possetti, M Muller, and J L Fabris, "Influence of the surrounding refractive index on the thermal and strain sensitivities of

a cascaded long period grating", Measurement Science And Technology, 18, pp. 3111–3116, (2007).

[78] Z. Tian, S. S. Yam, and H. Loock,"Single-Mode Fiber Refractive Index Sensor Based on Core-Offset Attenuators", IEEE Photonics Technology Letters, 20, 16, pp. 1387-1389, (2008).

[79] P. Lu, L. Men, K. Sooley, and Q. Chen, "Tapered fiber Mach–Zehnder interferometer for simultaneous measurement of refractive index and temperature", Applied Physics Letters, 94, 13, 1110, 1-3, (2009).

[80] J Wang and D Dai, "Highly sensitive Si nanowire-based optical sensor using a Mach–Zehnder interferometer coupled microring", Optics Letters, 35, 24, pp. 4229-4231, (2010).

[81] J. Yang, L. Jiang, S. Wang, B. Li, M. Wang, H. Xiao, Y. Lu, and H. Tsai, " High sensitivity of taper-based Mach–Zehnder interferometer embedded in a thinned optical fiber for refractive index sensing", Applied Optics, 50, 28, pp. 5503-5507, (2011).

[82] J. Yang, L. Jiang, S. Wang, Q. Chen, B. Li, and H. Xiao, "Highly Sensitive Refractive Index Optical Fiber Sensors Fabricated by a Femtosecond Laser", IEEE Photonics Journal, 3, 6, pp. 1189-1197 ,(2011).

[83] L. Huang, G. Lin, M. Fu, H. Sheng, H. Sun, and W. Liu, " A Refractive-index Fiber Sensor by Using No-Core Fibers", In Proceedings of the 2013 IEEE International Symposium on Next-generation Electronics, Kaohsiung, Taiwan, 25–26 February, pp. 100-102, (2013).

[84] C. Chen, C. Hsu, P. Huang, J. Wang, and W. Wu, "Optical Coupling Structures of Fiber-Optic Mach-Zehnder Interferometers Using CO2 Laser Irradiation", 2014,ID 938693, pp. 1-9, (2014).

[85] Z. Liu, Z. Tan, B. Yin, Y. Bai, and S. Jian, "Refractive index sensing characterization of a singlemode–claddingless–singlemode fiber structure based fiber ring cavity laser", Optics Express, 22,5, pp. 5037-5042, (2014).

[86] H. Luo, Q. Sun, Z. Xu, W. Jia, D. Liu, and L. Zhang, " Microfiber-Based Inline Mach–Zehnder Interferometer for Dual-Parameter Measurement ", IEEE Photonics Journal, 7,2, ID 7100908 , pp. 1-8, (2015).

[87] X. Bai, H. Wang, S. Wang, S. Pu, and X. Zeng, "Refractive index sensing characteristic of single-mode-multimode-single-mode fiber structure based on self-imaging effect", Optical Engineering, 54, 10, ID 106103, pp. (1-6), (2015).

[89] Q. Wang, L. Kong, Y. Dang, F. Xia, Y. Zhang, Y. Zhao, Haifeng Hu, and J. Li, "High sensitivity refractive index sensor based on splicing points tapered SMF-PCF-SMF structure Mach-Zehnder mode interferometer" Sensors and Actuators B: Chemical, 225, pp. 213-220, (2015).

[90] Q. Wang, W. Wei, M. Guo, and Y. Zhao, "Optimization of cascaded fiber tapered Mach–Zehnder interferometer and refractive index sensing technology", Sensors and Actuators B, 222, pp. 159–165, (2016).

[91] H. Dong, L. Chen, J. Zhou, J. Yu, H. Guan, W. Qiu, J. Dong, H. Lu, J. Tang, W Zhu, Z. Cai, Y. Xaio., J. Zhang, And Z. Chen, "Coreless side-polished fiber: a novel fiber structure for multimode interference and highly sensitive refractive index sensors", Optics Express, 25, 5, pp. 5352-5365,(2017).

[92] Q. Wang, B. Wang, L. Kong, and Y. Zhao, "Comparative Analyses of Bi-Tapered Fiber Mach–Zehnder Interferometer for Refractive Index Sensing", IEEE Transactions on Instrumentation and Measurement, 66,9, pp. 2483-2489, (2017).

[104] N. A. Salman, "Photonic Crystal Fiber Interferometer Based on Refractive Index Sensor ", M.SC thesis, Institute of Laser for Postgraduate Studies, University of Baghdad, (2017).

[93] C. F. Snyder and A. T. Hattenburg, "Refractive Indices and Densities of Aqueous Solutions of Invert Suger", United states Department of Commerce, national bureau of standard, (1963).

 [94] J. E. SAUNDERS, C. SANDERS, H. CHEN, and H. LOOCK, "Refractive indices of common solvents and solutions at 1550 nm", Applied Optics, 55, 4, pp. 947-953, (2016).

Appendix (A)

BOA 1004: C-band Booster Optical Amplifier

7.1.2.SP.1004 Rev D

Description

The BOA 1004 is a high saturation output power high bandwidth polarization maintaining Booster Optical Amplifier (BOA). It incorporates a highly efficient InP/InGaAsP Quantum Well (QW) layer structure and a reliable ridge waveguide design.

It is housed in a standard 14 pin butterfly package with integrated thermoelectric cooler and thermistor. Packaging options include isolator(s) and choice of single mode fiber and polarization maintaining fiber tails.
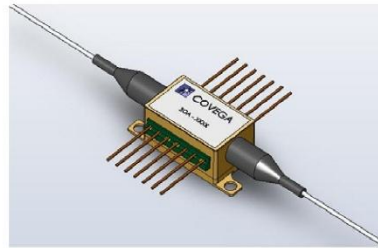
Applications

✓ Telecom & Datacom
✓ Booster Amplifier of Fixed and Tunable ITU Lasers and Transmitters
✓ Research & Non-Linear Applications

Features

→ High Saturation Output Power
→ Broad Spectral Bandwidth
→ High Fiber-to-Fiber Gain
→ High Polarization Extinction Ratio

Specifications

CW; T (Chip) = 25°C, T (Case) = 0 - 70°C

Parameter		Min	Typ	Max	
Operating Current	I_{OP}		600	750	mA
Central Wavelength	λ_C	1530	1550	1570	nm
Optical 3 dB Bandwidth	BW	90	100		nm
Saturation Output Power @ -3 dB	P_{SAT}	13	15		dBm
Small Signal Peak Gain @ Pin = -20 dBm	G	25	28		dB
Gain Ripple (rms) @ I_{OP}	δG		0.1	0.2	dB
Noise Figure	NF		7	9	dB
Forward Voltage	V_F		1.4	1.6	V
TEC Operation (typ / max @ T_{CASE} = 25°C / 70°C)					
- TEC Current	I_{TEC}		0.12	1.5	A
- TEC Voltage	V_{TEC}		0.25	4	V
- Thermistor Resistance	R_{TH}		10K		Ω
SPECIFICATIONS SUBJECTED TO CHANGE WITHOUT NOTICE					

COVEGA

BOA 1004

Performance

Packaging


```
PIN IDENTIFICATION

1.  TEC +        14.  TEC -
2.  Thermistor   13.  Case
3.  NC           12.  NC
4.  NC           11.  SOA Cathode
5.  Thermistor   10.  SOA Anode
6.  NC            9.  NC
7.  NC            8.  NC

Recommended mounting torque is
10-20oz.in ( 0.07-0.14N.m ).
```

all dimensions in mm
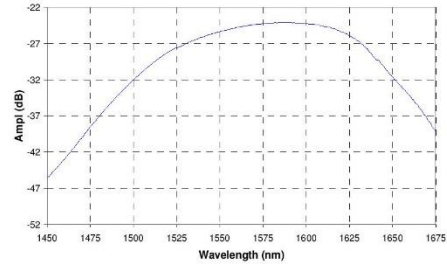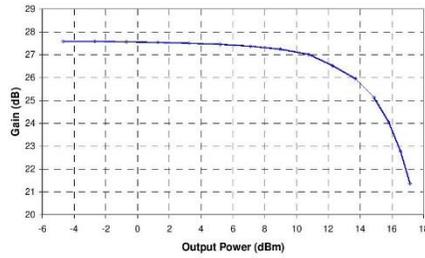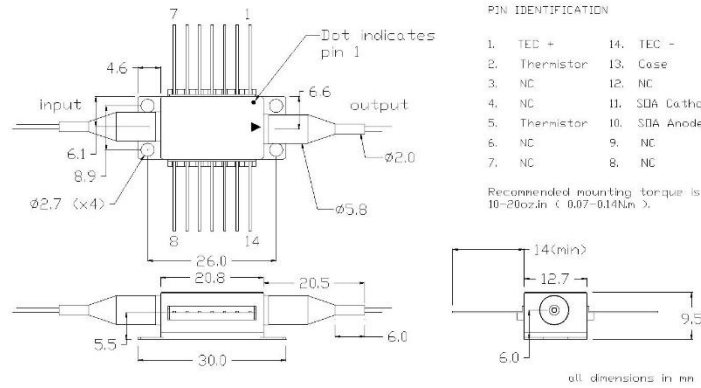
Ordering Information

BOA 1004 - X - 0 - X - X - X - X - X

X	0	X	X	X	X	X	Numeric
Isolator	**Reserved**	**Fiber jacket configuration***	**Input Fiber**	**Output Fiber**	**Input Connecter**	**Output Connecter**	**Grade Level**
0 = none		T = SMF-28, tight jacket	S = SMF	S = SMF	A = FC/APC	A = FC/APC	0 / blank = Std.
1 = input only		V = PMF 1550 nm, loose tube	P = PMF	P = PMF			1 = XL
2 = output only							2 = Reserved
3 = input & output							
Custom orders with isolators require a minimum purchase quantity.							
* see all of the fibertail options in the Covega catalog							

Appendix (B)

Light

▼ **CHAPTERS**

Coherent
Sources
Incoherent
Sources
Quantum
Electronics

Drivers/Mounts

Accessories

▼ **SECTIONS**

Laser Diode
Controllers
Temperature/TEC
Controllers
LD/TEC Controllers
LD/TEC Platforms

LD Mounts

LED Drivers

LED Mounts

For current pricing, please see our website.

Universal Butterfly Mount

The LM14S2 Butterfly Mount is designed to operate all lasers and two-port electro-optic devices in a 14-pin butterfly package. The top surface includes heat sink fins and a recessed region to mount the laser diode, resulting in a very low-profile package. The LM14S2 includes a laser diode TEC lockout feature, which disables the laser when the TEC controller is not active.† This mount is designed to allow up to 5 A of laser current and 5 A of TEC current. It also provides a Zero Insertion Force (ZIF) Socket, a remote interlock connection, and an LED to indicate when the laser diode is enabled.

LM14S2

This package comes with two adapter cards, each plugging into the connector at the bottom of the mount (see section below for details). A Bias-T Adapter is also included with the product, allowing for RF modulation of butterfly lasers specifically designed with this capability. The LM14S2 is pin-for-pin compatible with all Thorlabs' Benchtop Laser Diode Controllers (see pages 1436 - 1439), eliminating the need for custom-made interface cables.

† TEC lockout, which is easily bypassed if not required, only functions with Thorlabs' lasers and TEC controllers (see pages 1436 - 1480). The TEC controller requires that the laser package has an integrated TEC and thermal sensor.

Features

- Compatible with all Commercially Available Laser Modules and Two-Port Electro-Optic Devices in 14-Pin Butterfly Packages
- Zero Insertion Force (ZIF) Sockets
- Compatible with Thorlabs' Laser Diode and TEC Controllers (See Pages 1436 - 1480)
- Compact, Low-Profile Design
- TEC Lockout Protection Circuit

PARAMETER	VALUE
Maximum Laser Current	5 A
Polarity of Laser Diode	AG
Polarity of Monitor Diode	Floating
Maximum TEC Current	5 A
Temperature Sensor	Thermistor
Temperature Range*	0 to 70 °C
Temperature Coefficient of Heat Sink	3 °C/W
Dimensions	3.5" x 3.5" x 1.25" 88.7 mm x 88.9 mm x 31.8 mm

*At 25 °C with 2 A TEC current, integrated into laser package. Laser Diode dependent.

LM14S2
Shown with a Two Port Electro-Optic Device

+**Mechanical**
Drawings Available on the
WEB
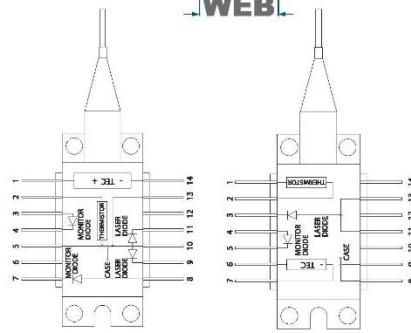
Type 1
Pump Laser Diode*

Type 2
Telecom Laser Diode*

*View shows alternate locations for monitor and laser diodes

Adapter Cards for Custom PIN Configuration

The LM14S2 eliminates the restriction of fixed pin configurations by using swappable configuration cards that plug into a connector located on the bottom of the mount. Two cards are included with the LM14S2. One card is pre-configured for both Type 1 and Type 2 lasers. The second card is a user-configurable card (LM14S2-UA) designed to allow custom wiring of the mount.

LM14S2
Universal Adapter Card

PIN #	CONNECTOR (TYPE 1)	CONNECTOR (TYPE 2)
1	TEC Anode	Thermistor Ground
2	Thermistor	Thermistor
3	PD Anode	LD Cathode (DC)
4	PD Cathode	PD Anode
5	Thermistor Ground	PD Cathode
6	N.C.	TEC Anode
7	PD Cathode	TEC Cathode
8	PD Anode	LD Anode, Ground
9	LD Cathode	LD Anode, Ground
10	LD Anode, Ground	N.C.
11	LD Cathode	LD Anode, Ground
12	N.C.	LD Cathode (RF)
13	LD Anode, Ground	LD Anode, Ground
14	TEC Cathode	N.C.

ITEM #	$	£	€	RMB	DESCRIPTION
LM14S2	$ 324.00	£ 233.28	€ 281.88	¥ 2,582.28	Universal 14-Pin Butterfly Laser Diode Mount
LM14S2-UA	$ 29.00	£ 20.88	€ 25.23	¥ 231.13	LM14S2 Universal Adapter Card for Custom Pin Configuration

Appendix (C)

THORLABS

Laser Diode Controller

LDC200C Series
Operation Manual

2014

General Information

The Thorlabs LDC200C Series Laser Diode Controllers are high accuracy precise injection current controllers for laser diodes and LEDs. Together with a Thorlabs Temperature Controller a stable operation of the connected laser diode can be achieved. The LDC200C Series includes the following types:

- LDC200CV - designed for safe operation of VCSEL laser diodes.
- LDC201CU - ultra low noise current (<0.2µA RMS).
- LDC202C, LDC205C and LDC210C - enhanced compliance voltage (>10V) for use with blue laser diodes.
- LDC240C - higher current (4A).

The LDC200C Series controllers are easy to operate via the operating elements on the front panel. Operating parameters are shown on a 5-digit LED display. UP-DOWN keys allow to select the parameter to be displayed.

After switching on a LDC200C Series laser diode controller, it remains in LASER OFF mode. The laser current can be switched on/off using the appropriate key at the front panel.

Additionally the laser current can be switched by applying a TTL signal to the LD remote input at the rear of the unit.

The laser and the photodiode are connected via a 9-pin D-SUB jack at the rear of the unit. The output for the laser diode and the input for the photodiode are bipolar, thus all polarities of commercial available laser diodes can be connected.

The injection current or the optical output power of the laser diode can be modulated applying a modulation signal to the input at the rear of the unit.

A voltage proportional to the laser diode current is provided for monitoring purposes at an analog control output at the rear.

If an error occurs or the limit for the laser current is reached, the corresponding LED lights up and a short beep gives a warning.

For a low ripple and noise of the output current a mains filter is installed and the transformer is shielded carefully.

The LDC200C Series controller are cooled by an internal fan, which protects the unit against overheating in case of high environmental temperatures. With free air circulation a safe operation of the unit is guaranteed up to 40 °C ambient temperature.

Warning

Do not obstruct the air ventilation slots in the housing!

Note

In order to prevent damages to the laser diode, it is recommended to mount the laser into a suitable Thorlabs laser diode mount and connect it to the LDC200C Series using the supplied Thorlabs CAB400 cable. This ensures the utmost protection of the laser diode from damage by wrong connection.

Appendix (D)

THORLABS

Thermoelectric Temperature Controller

TED200C
Operation Manual

2011

General Information

The thermoelectric Temperature Controller TED200C by Thorlabs is an extremely precise temperature controller for laser diodes and detectors.

The TED200C is excellently suited for:

- **wavelength stabilization of laser diodes**
- **noise reduction of detectors**
- **wavelength tuning by regulating the temperature**
- **modulation of wavelength by tuning the temperature**

The unit is easy to use due to the clearly arranged operating elements on the front panel. The operating parameters are shown by a 5-digit LED display, the measurement value shown is selected via keys.

The gain (P-share), the integral share and the derivative share of the PID temperature control loop can be set independent of each other.

Different temperature sensors can be used with the temperature controller TED200C, thermistors, or temperature IC sensors: AD590, AD592, LM135, LM 335. With a thermistor the temperature display is shown as resistance value in kΩ, if the TED200C is operated with a temperature sensor IC the temperature is shown in °C.

The output for the TEC current can be switched on or off via key from the front panel.

The temperature sensor and the TEC element are connected by a 15-pin D-sub jack at the rear of the unit.

At the output jack a control signal is available to drive an external LED to indicate TEC ON mode when the TEC current loop is activated.

The set value of the temperature can be changed with a knob at the front panel or via an analog input at the rear of the unit.

An analog voltage proportional to the actual value of the temperature is available at the rear of the unit for monitoring purposes.

The unit has been designed for safe operation with environmental temperatures of more than 40 °C provided that a free air circulation through the ventilation slots at the rear and at both sides of the unit is maintained.

Attention

Do not obstruct the air-ventilation slots in the housing!

In case of overheating caused by too high environmental temperatures or closed ventilation slots the unit automatically switches the output off to avoid damages.

The LED "OTP" (over-temperature-protection) indicates the over-temperature.

After temperature drop of about 10 °C the LED "OTP" extinguishes and the output current can be switched on again by pressing the key "ON".

If an error occurs (OTP or OPEN) the corresponding LED lights up and a beeper gives a short warning signal.

Appendix

(E)

Corning® SMF-28® Ultra Optical Fiber
Product Information

CORNING

Corning® SMF-28® Ultra optical fiber is an ITU-T Recommendation G.652.D compliant optical fiber with Corning's enhanced low-loss and bend fiber technologies. This full-spectrum fiber has bend performance that exceeds the ITU-T Recommendation G.657.A1 standard and still splices the same as the installed base of standard single-mode fibers such as SMF-28e+ fiber. SMF-28 Ultra fiber offers industry-leading specifications for attenuation, macrobend loss, and polarization mode dispersion values, which provide a solid foundation for new network deployments as well as upgrades to existing networks. Since Corning brought the first fiber to market more than 40 years ago, Corning's leadership in single-mode fiber innovation has been unparalleled.

Optical Specifications

Maximum Attenuation

Wavelength (nm)	Maximum Value* (dB/km)
1310	≤ 0.32
1383**	≤ 0.32
1490	≤ 0.21
1550	≤ 0.18
1625	≤ 0.20

* Alternate attenuation offerings available upon request.
** Attenuation values at this wavelength represent post-hydrogen aging performance.

Attenuation vs. Wavelength

Range (nm)	Ref. λ (nm)	Max. α Difference (dB/km)
1285 – 1330	1310	0.03
1525 – 1575	1550	0.02

The attenuation in a given wavelength range does not exceed the attenuation of the reference wavelength (λ) by more than the value α.

Macrobend Loss

Mandrel Radius (mm)	Number of Turns	Wavelength (nm)	Induced Attenuation* (dB)
10	1	1550	≤ 0.50
10	1	1625	≤ 1.5
15	10	1550	≤ 0.05
15	10	1625	≤ 0.30
25	100	1310, 1550, 1625	≤ 0.01

*The induced attenuation due to fiber wrapped around a mandrel of a specified radius.

Point Discontinuity

Wavelength (nm)	Point Discontinuity (dB)
1310	≤ 0.05
1550	≤ 0.05

Cable Cutoff Wavelength (λ_{cc})

$\lambda_{cc} \leq 1260$ nm

Mode-Field Diameter

Wavelength (nm)	MFD (μm)
1310	9.2 ± 0.4
1550	10.4 ± 0.5

Dispersion

Wavelength (nm)	Dispersion Value [ps/(nm·km)]
1550	≤ 18.0
1625	≤ 22.0

Zero Dispersion Wavelength (λ_O): 1304 nm ≤ λ_O ≤ 1324 nm
Zero Dispersion Slope (S_O): $S_O \leq 0.092$ ps/(nm²•km)

Polarization Mode Dispersion (PMD)

	Value (ps/√km)
PMD Link Design Value	≤ 0.04*
Maximum Individual Fiber PMD	≤ 0.1

*Complies with IEC 60794-3: 2001, Section 5.5, Method 1, (m = 20, Q = 0.01%), September 2001.

The PMD link design value is a term used to describe the PMD of concatenated lengths of fiber (also known as PMD_Q). This value represents a statistical upper limit for total link PMD. Individual PMD values may change when fiber is cabled.

Dimensional Specifications

Glass Geometry

Fiber Curl	≥ 4.0 m radius of curvature
Cladding Diameter	125.0 ± 0.7 µm
Core-Clad Concentricity	≤ 0.5 µm
Cladding Non-Circularity	≤ 0.7%

Coating Geometry

Coating Diameter	242 ± 5 µm
Coating-Cladding Concentricity	< 12 µm

Environmental Specifications

Environmental Test	Test Condition	Induced Attenuation 1310 nm, 1550 nm, and 1625 nm (dB/km)
Temperature Dependence	-60°C to +85°C*	≤ 0.05
Temperature Humidity Cycling	-10°C to +85°C up to 98% RH	≤ 0.05
Water Immersion	23°C ± 2°C	≤ 0.05
Heat Aging	85°C ± 2°C	≤ 0.05
Damp Heat	85°C at 85% RH	≤ 0.05

*Reference temperature = +23°C
Operating Temperature Range: -60°C to +85°C

Mechanical Specifications

Proof Test

The entire fiber length is subjected to a tensile stress ≥ 100 kpsi (0.69 GPa).*
*Higher proof test levels available.

Length

Fiber lengths available up to 63.0 km/spool.

Performance Characterizations

Characterized parameters are typical values.

Core Diameter	8.2 µm
Numerical Aperture	0.14 NA is measured at the one percent power level of a one-dimensional far-field scan at 1310 nm.
Effective Group Index of Refraction (N_{eff})	1310 nm: 1.4676 1550 nm: 1.4682
Fatigue Resistance Parameter (N_d)	20
Coating Strip Force	Dry: 0.6 lbs. (3N) Wet, 14-day room temperature: 0.6 lbs. (3N)
Rayleigh Backscatter Coefficient (for 1 ns Pulse Width)	1310 nm: -77 dB 1550 nm: -82 dB

CORNING

Appendix

(F)

THORLABS

Coreless Termination Fiber

FG125LA
FG250LA
FG400LA

Description

These coreless silica termination fibers can be spliced to the ends of standard fiber to reduce back reflections or prevent damage to the fiber end face. A return loss of greater than 65 dB is achieved by splicing 0.25 m of coreless fiber to the desired component.

Specifications

Specifications			
Item #	FG125LA	FG250LA	FG400LA
Wavelength Range	400 - 2400 nm		
Return Loss	>65 dB with 0.25 m		
Glass Diameter	125 ± 1 µm	250 ± 10 µm	400 ± 15 µm
Coating Diameter	250 µm ± 5%	400 ± 20 µm	550 ± 20 µm
Coating	Acrylate		
Glass Refractive Index	1.467287 @ 436 nm 1.458965 @ 589.3 nm 1.450703 @1020 nm 1.444 @1550 nm		
Operating Temperature	-40 to 85 °C		
Proof Test Level	>100 kpsi		
Recommended Stripping Tool	T06S13 or FTS4	T12S16	T18S25

Appendix

(G)

Specifications to arc fusion splicer (FSM-60S)

Item	Specifications
Applicable fibers	SMF ,MMF ,DSF ,NZDSF etc.
Cladding dia./sheathe dia.	80 to150 µm / 100 to 1000 µm
Splice mode	Total 100 modes
Automatic fiber identification	SMF ,MMF ,NZDSF
Splice loss estimate	Equipped
Attenuation splice	0.1 dB to 15dB by 0.1 dB step
Splice result storage	Last 2000 splices
Viewing methods	2 axis 2CMOS camera with 4.1 LCD
Tension test	1.96 to 2.25 N
Protection sleeve	60mm ,40mm and Fujikura micro sleeves
Diagnostic function	Equipped

الخلاصة

أجهزة قياس التداخل تستخدم على نطاق واسع في تطبيقات التحسس. في هذا العمل، تم تصنيع متحسس بسيط بالاعتماد على تداخل ماخ زيندر من الألياف البصرية بالكامل على أساس طريقة اللحام غير المتوافق مع الانماط، لاستشعار تغير معامل الانكسار / التركيز . لقد تم دراسة تأثير طول وقطر الألياف عديمة القلب كمعلمات فعالة لتحسين حساسية جهاز التحسس. أن تصميم وتصنيع أجهزة الاستشعار تنطوي على عملية قطع ولحام قطعة من الليف البصري عديم القلب مع جزأين من الألياف البصرية احادية النمط. في هذا التركيب تعتبر قطعة الليف البصري عديمة القلب بمثابة شريحة التحسس. أن مصدر توليد النطاق العريض تم ربطه بنهاية التركيب من جهة ، بينما كانت الجهة الاخرى متصلة بمحلل الطيف البصري لرصد التغير في الطيف.

تم استخدام ثلاثة أطوال مختلفة (2، 4، و 6 سم) من الليف خالي القلب لإجراء التجارب. كان قطر الليف خالي القلب عند 125 ميكرون حيث وجد أن حساسية المستشعر ليس لديها تغير ملحوظ مع تلك الأطوال عندما يبقى قطر الليف ثابتا على 125 ميكرون. تم اجراء التقشير باستخدام حامض الهايدروفلورايد 40٪ للتقليل من قطر الليف عديم القلب

لقد وجد أن حساسية جهاز الاستشعار تم تحسينها عن طريق تقليل قطر الليف عديم القلب بالتقشير باستخدام حامض الهايدروفلورايد 40٪ لمدة 40 دقيقة. وكانت أقصى تحسس تم الحصول عليه هي 340.89 نانومتر /وحدة معامل الانكسار في المواد ذات معاملات انكسار مختلفة (الهواء والماء والأسيتون، و N- الهكسان) عندما تقليل قطرها إلى 60 ميكرون.

وكان الحد الأقصى للتحسس التي تم الحصول عليها هي 0.52 نانومتر /٪ (بتوافق مع قابلية الفصل بين الاطوال الموجية من 0.038٪ في قابلية الفصل للجهاز عند الطول الموجي لمحلل الطيف البصري من 0.02 نانومتر) عندما تراوحت مجموعة تركيز محلول السكروز من 0 إلى 60٪ في القطر وطول CF من 60 ميكرون و 2 سم على التوالي.

تم اجراء دراسة نظرية لتغير قطر الليف عديم القلب وتأثيره على النمط الاساسي والانماط عالية الرتبة باستخدام برنامج المحاكاة الفيزيائي Multiphysics COSOL 5.2a وظهر كلما تم تقليل قطر الليف عديم القلب تنحصر الانماط بصورة اكبر وافضل بفعل الموجات الهاربة تكون اكثر تفاعلاً مع تغير معامل الانكسار للمحيط الخارجي.

متحسس معامل الانكسار مبني على تركيبة مدخال ماخ زيندر ذي الليف عديم القلب

رسالة مقدمة إلى

معهد الليزر للدراسات العليا /جامعة بغداد /لاستكمال متطلبات نيل شهادة ماجستير علوم في الليزر/ هندسة الكترونيك واتصالات

مـن قبـل

سيف عقيل محمد

بكالوريوس هندسة ليزر والكترونيات بصرية -2008

باشراف

الأستاذ الدكتور عبد الهادي مطشر عبد

1439 هـ   **2017 م**